VDE-SAT Ranging for Critical Navigation

Characteristics of Experimental VDE-SAT Ranging Signals and System Performance Analysis for Critical Navigation

Øyvind Bryhn Pettersen

Delft University of Technology

VDE-SAT Ranging for Critical Navigation

Characteristics of Experimental VDE-SAT Ranging Signals and System Performance Analysis for Critical Navigation

by

Øyvind Bryhn Pettersen

to obtain the degree of Master of Science
at the Delft University of Technology,
to be defended publicly on Tuesday November 21, 2023 at 09:00 AM.

Student number:	4810511	
Project duration:	February 10, 2023 – November 21, 2023	
Thesis committee:	Dr. ir. J.A.A. van den IJssel,	TU Delft, supervisor
	Dr. ir. E.J.O. Schrama,	TU Delft, committee chair
	Dr. S.M. Cazaux,	TU Delft, external committee member
	Ir. S.I. Rasmussen,	Space Norway, external supervisor

Cover: View from space by NASA; render of NorSat-TD by UTIAS Space Flight Laboratory

TU Delft

Preface

Here is my final product, after five wonderful years at the TU Delft. Thanks for taking a look at it. It took five years to make this, not because it is a particularly long report, but rather because education is a painstakingly slow and monumental effort. It is done in steps, not leaps. Now, I have finally done the distance, and could not be more proud to have reached the end of this walk. Thanks for all the learning along the way.

The past year I have been given the unique opportunity to work directly on the development of critical infrastructure for my home, Norway. I have also been so lucky to do this together with an excellent group of people. First, a great big thanks to my thesis supervisor Jose. You have been an invaluable support, a pragmatic cliff where I could rest all of my concerns, while keeping a sharp eye out to bring out the best of this thesis. Thanks for taking on the challenge with me.

Thank you to Sven-Ingve for the leadership over the past couple of years. Thank you so much for believing in me when I stepped into your office with the idea of doing a thesis together, it has given me opportunities I will be forever grateful for. By extension, thanks to everyone at Space Norway for the very warm welcome at your offices.

And of course, the ones who make it all possible: Thank you to all my friends for the support, every day. That's to my new, now old, friends in Delft, and my old, still old, friends waiting for me in Norway. I am all at once equally heartbroken to be leaving, and elated to get started in Oslo. A special thanks to everyone at the VSV 'Leonardo da Vinci', for giving me an arena to develop myself - and memories for a lifetime.

Finally, my dear family, for your love and encouragement every step of this long walk. Thanks for instilling confidence and independence in me growing up, for always telling me I could, even when I probably couldn't, and ensuring that home was always there for me when I was ready to return. The very biggest thanks to my sister and best friend, Ingeborg.

Øyvind Bryhn Pettersen
Delft, October 2023

Contents

Nomenclature

The nomenclature contains the complete list of symbols and abbreviations for both the thesis report and journal article. Due to the appended journal article, formatting differences between the nomenclature and article may occur.

List of Abbreviations

AD	Anderson-Darling
AIS	Automatic Identification System
BPSK	Binary phase-shift keying
C/A	Coarse acquisition
CDDIS	Crustal Dynamics Data Information System
Corr.	Correction
CRC	Cyclic redundancy check
DOP	Dilution of precision
DSSS	Direct-sequence spread spectrum
ECEF	Earth-centred, Earth-fixed
Elev.	Elevation angle
ENU	East-North-Up
ESA	European Space Agency
GDOP	Geometric dilution of precision
Geom.	Geometric
GIM	Global Ionosphere Map
GNSS	Global Navigation Satellite System
GPS	Global Positioning System
GSSC	GNSS Science Support Centre
HDOP	Horizontal dilution of precision
IALA	International Association of Marine Aids and Lighthouse Authorities
ICING	Independent Critical Navigation
IGS	International GNSS Service
ITU	International Telecommunications Union
KS	Kolmogorov-Smirnov
LEO	Low-Earth orbit
NAVISP	Navigation Innovation and Support Program
Param.	Parameter
Perf.	Performance
PNT	Position, navigation and timing
Pos.	Position
PPS	Pulse-per-second
PR	Pseudorange
PRN	Pseudo-random noise
R-mode	Ranging mode
RSS	Residual sum of squares
SE	Standard error
SNR	Signal-to-noise ratio
St. dev.	Standard deviation
Std. err.	Standard error
STEC	Slant total electron count
Stud.	Studentized
TD	Technology demonstrator
TEC	Total electron count
UTC	Coordinated universal time
VDE-SAT	VDES satellite component
VDE-TER	VDES terrestrial component
VDES	VHF Data Exchange System
VHF	Very High Frequency

List of Symbols

β	Model parameter
Δt	Measured time offset
δt	Relative time offset
δt_r	Receiver clock offset

δt_t	Transmitter clock offset
$\delta \rho_\epsilon$	All non-clock errors in pseudorange
ϵ_r	Error in geometric range estimate
$\hat{y}$	Estimated response
$\hat{\beta}$	Estimated model parameter
$\hat{\mathbf{r}}_r$	Estimated receiver position
$\mathbf{E}$	ECEF reference frame
$\mathbf{f}$	Function
$\mathbf{H}$	Design matrix
$\mathbf{J}$	Jacobian matrix
$\mathbf{K}$	Geometric factor matrix
$\mathbf{r}_\mathbf{t}^*$	Corrected satellite position
$\mathbf{r}_\mathbf{t}^{\text{TEL}}$	Satellite position from telemetry
$\mathbf{r}_\mathbf{t}$	Satellite position
$\mathbf{R}$	Rotation matrix
$\mathbf{v}_\mathbf{t}^{\text{TEL}}$	Satellite velocity from telemetry
$\mathbf{v}_\mathbf{t}$	Satellite velocity
$\mathbf{x}$	Estimated state
ω_e	Earth angular rotation rate
Φ	Sum of squared residuals
ρ	Geometric range
ρ^*	Corrected range
ρ_1	C/A pseudorange
ρ_2	L5-band pseudorange
ρ_{true}	True geometric range
ρ_c	Ionosphere-free pseudorange
σ	Standard deviation
$\text{Cov}(\mathbf{x})$	Position covariance matrix
$\text{Cov}(\rho)$	Observation covariance matrix
θ	Dynamic parameters
$\tilde{\rho}$	Pseudorange
A	Final combined set
c	Speed of light in a vacuum
D	Diagonal element of geometric factor matrix
$d_{\text{I}_g r}$	Ionospheric group delay
e_ρ	Pseudorange residual
E_c/N_0	Carrier-energy-to-noise ratio
E_s/N_0	Signal-to-noise ratio
f	Frequency
f	Least-squares residual
f_1	C/A-code frequency
f_2	L5-band frequency
N	Navigation set
N	Variable number of observations
n	Number of observations
O	Observation set
p	Number of parameters
R^2	R^2-metric
S_n	VDES slot number
T	Telemetry set
t	Time
t	t-statistic
t_r	Time of reception
t_t	Time of transmission
X	Predictor
x	Observed predictor
X_{ECEF}	X-coordinate in ECEF-frame
Y	Response
y	Observed response
Y_{ECEF}	Y-coordinate in ECEF-frame
Z_{ECEF}	Z-coordinate in ECEF-frame

1 Introduction

This introduction will provide a broader look at the problem that is central in the journal article in chapter 2. It is necessary to first understand the technical background presented in this introduction to understand the methods and conclusions of the article. First, the need for reliable PNT in the Arctic and the contemporary threats to the current system is presented in section 1.1. Further, a brief overview of the applicability of the VHF (Very High Frequency) Data Exchange System (VDES) to the problem, as well as a required technical overview of the system is given in section 1.2. Prior research on the topic of alternative sources of position, navigation and timing (PNT), leading up to VDES ranging as a PNT-source, is presented in section 1.3. Finally, the research objective, highlighted sub-goals, and a short overview of the applied methods for this thesis project are given in section 1.4.

1.1. PNT in the Arctic

The requirements for continuously available PNT become ever more demanding in a growing and digitalizing maritime industry. In the northern regions of Norway, PNT information is essential for critical infrastructure: navigation of shipping routes, search & rescue and medical evacuation, and air traffic control. These critical services are under threat in conditions where Global Navigation Satellite Systems (GNSS) are unavailable, which in the same northern regions are becoming increasingly common, and are now a nearly daily occurrence which can affect the safety of those living in the far-North[1][2][3]. Intentional and unintentional disturbances of GNSS in the Arctic drive the need for an alternative system to ensure the continuation of critical operations when GNSS becomes unavailable.

There are three primary reasons for the limited GNSS availability in the Arctic. All large GNSS constellations are designed with their primary goal of covering the mid-latitudes, meaning the orbital inclinations of these constellations are typically 60°. This results in no satellite passes over the polar regions, illustrated in Figure 1.1, and subsequently GNSS observations become more rare, and are only available at lower elevation angles for users in the Arctic. Similarly, GNSS augmentation systems are typically based on Geostationary orbits, causing limited coverage for users above 75° latitude (De Jong et al., 2014). Further, the International Association of Marine Aids and Lighthouse Authorities (IALA) recommendation R0129 on GNSS vulnerability describes how "jamming of GNSS signals can be achieved quite easily using relatively low-cost equipment" (IALA, 2012b, p. 7). This issue is further accelerated in the Arctic where signal power levels are lower due to the required long propagation of signals to the user. Additionally, the Arctic is a region of high ionospheric scintillation, which causes a reduction in accuracy and has also been correlated with loss of the signal entirely (Aquino et al., 2005). Poor PNT-coverage, intentional jamming of low-power signals, and ionospheric scintillation add up to the contemporary issue of limited GNSS availability in the Arctic, particularly affecting users in Northern Norway.

A primary mitigation to the issue of poor PNT-coverage in the Arctic is answered by the growing interest in low-Earth orbit (LEO) satellite constellations. The geometry of these constellations can

[1]URL https://www.nrk.no/tromsogfinnmark/kraftig-okning-av-gps-jamming-over-finnmark-1.16309499, Accessed 3/10/2023.
[2]URL https://www.nrk.no/tromsogfinnmark/mangedobling-av-gps-jamming-mot-norge-1.16563000, Accessed 3/10/2023.
[3]URL https://www.tv2.no/nyheter/innenriks/ambulansefly-kunne-ikke-lande-etter-gps-utfall/10397144/, Accessed 3/10/2023.

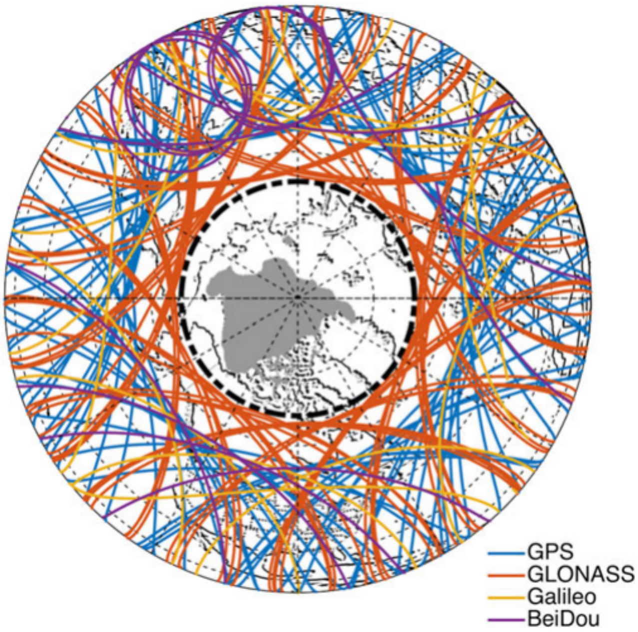

Figure 1.1: Visualized ground tracks of all major GNSS constellations over the North Pole (Reid et al., 2016, Fig. 14)

directly respond to the primary concerns presented above. More constellations of LEO satellites are being proposed every year, with large-scale constellations like Iridium NEXT, and OneWeb providing global coverage, including polar areas (Maine et al., 1995; de Selding, 2015). An added benefit of LEO constellations is also the significantly closer proximity to the user, meaning possibly higher received power levels at the user. For Iridium, the path attenuation of a transmitted signal has shown to be up to 30 dB less at the receiver than for GPS (Reid et al., 2020, p. 1364). Modern satellite constellations could thus provide a benefit to the issue of poor PNT-coverage in the Arctic.

1.2. VHF Data Exchange System

Developments in the digitized maritime industry may be a part of the solution to the problem of GNSS disturbances in the Arctic. Over the past decade, a new digital data exchange system, VDES, in the maritime frequency bands has been developed, enabling a transition to digitized operations at sea (Lázaro et al., 2019). VDES has allocated frequencies in the range of 156.025 - 162.025 MHz, a part of the marine VHF radio frequency band, and is an evolution of the Automatic Identification System (AIS). The need for digital data transmission channels in this frequency band has been recognised by the International Telecommunications Union (ITU), which has refined the VHF frequency band and defined channels for data transmission (IALA, 2019). Additional, technical specifications of VDES and its satellite component VDE-SAT have also been defined by the ITU (ITU-R, 2022). VDES builds on the mature AIS tracking system by providing means to a one- and two-way data exchange between ships, shore and satellites, as illustrated in Figure 1.2. With data exchange capabilities over alternative frequencies, it is possible that ranging application of VDES can form a robust contingency as PNT in the Arctic, resistant to the disturbances present at GNSS-frequencies. This section will briefly present the required technical information on VDES required for the technical analysis of the journal article in chapter 2.

A VDES packet is made up of frames, which again are defined by slots containing data (IALA, 2019). A frame is a 60 s transmission, equally divided into 2250 slots of approximately 26.667 ms, synchronized in time, using GNSS, to coordinated universal time (UTC) time. After a ramp up sequence, each slot contains a sync word, followed by the transmission Link ID specifying the channel configuration. Furthermore, a slot will contain the transmitted data, ending with a cyclic redundancy check (CRC), which is a form of error control where the bits of the transmitted message are interpreted as a high-degree polynomial and evaluated to a checksum (Sheng-Ju, 2015). This checksum is then re-

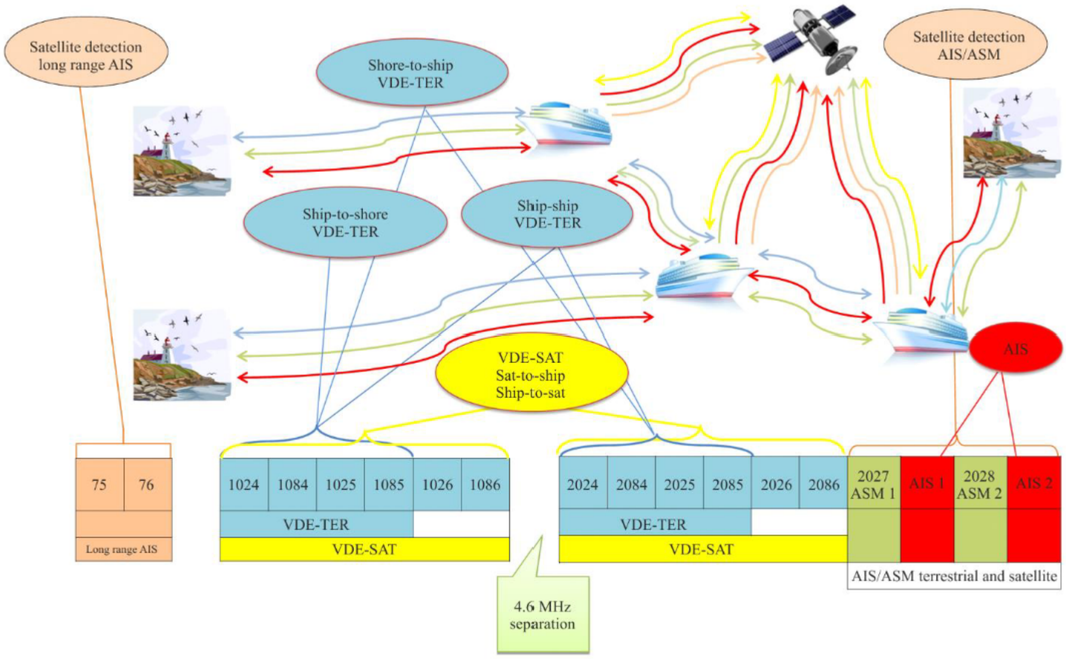

Figure 1.2: An illustration of the many communication channels available over VDES (ITU-R, 2022, Fig. 1).

evaluated at the receiver side to verify the received string of bits. Each slot will contain six repetitions of the (encoded) data and CRC which are combined at the receiver, meaning each data transfer has one associated checksum by CRC.

The physical layer channel defines key technical parameters for the transmitted signal. The VDE-SAT Link ID 29 is characterized by a 150 kHz bandwidth and a binary phase-shift keying (BPSK) modulation, transmitted over a frequency of 161.8625 MHz, near the upper limit of the VDES-band (ITU-R, 2022). The channel also incorporates a spread spectrum technique to double the bandwidth of the transmitted signal. This is done by a direct-sequence spread spectrum (DSSS) technique where the transmitted symbols are first modulated with a known spreading sequence with two chips per symbol, doubling the number of transmitted symbols. The results is a wider bandwidth for the transmitted signal, making it more resistant to interference and jamming (Kang et al., 2013).

This section has briefly presented details on VDES. The system context is established, and an overview of the system functionalities is presented and illustrated in Figure 1.2. Further, the technical details required to understand all aspect of the work in the journal article in chapter 2 are explained. This concerns largely the VDES packet structure and physical layer characteristics. With this information, all considerations regarding VDES in the journal article should be clear to the reader.

1.3. Prior research and ICING

Navigation using stray signals has been a topic of research for many decades. Often called ”signals of opportunity”, typically considered signals are stray cellular and now 5G signals, TV, Wi-Fi and even analogue audio transmission (Kapoor et al., 2017; Jia & Kassas, 2022; Kassas et al., 2022). The applications vary from direct navigation-aid to integrity monitoring of GNSS. Another signal that has been studied as a possible signal of opportunity, as a tool for ranging, is AIS.

The first developments of AIS Ranging mode (R-mode) was published in a 2009 plan from IALA with a proposal for its development as ground-based augmentation to GNSS (IALA, 2012a). Feasibility studies of AIS as a source of ranging signals followed the years after, with positive conclusion on the possible error level using ground-based signals of opportunity from AIS base stations (Johnson & Swaszek, 2014). Testbeds were built in the Baltic sea, and outside Dalian, in China, that verified the results of the feasibility studies (Hu et al., 2015; Gewies, 2018). At the same time, research on the same application to ground-based R-mode using the novel VDES, instead of AIS, showed a significant performance increase (Šafář et al., 2020). These results are also verified by test campaigns run in Germany (Wirsing et al., 2019). Later, statistical lower bounds of the performance of simulated ranging signals based on the satellite component of VDES, VDE-SAT, gave similarly positive conclusions for R-mode applications with LEO satellite systems (Šafář et al., 2021). The most recent and relevant literature give positive recommendations for the use of VDE-SAT as a possible augmentation to modern GNSS (Šafář et al., 2018; Owens et al., 2021).

There is no research in the field of VDE-SAT ranging considering signal propagation effects, nor empirical verification of VDE-SAT ranging performance. This knowledge gap was identified and resulted in the launch of the European Space Agency (ESA) project ICING[4] (Independent Critical Navigation), with the goal of testing a concept where VDES is used to provide purpose-designed ranging signals for critical navigation applications in the exposed GNSS-conditions of the Arctic. This is the first investigation into what could form the basis of a backup or contingency satellite navigation system for maritime users in polar regions. The ICING project is funded under the Navigation Innovation and Support Program (NAVISP), and conducted by a consortium with Space Norway as lead, and Kongsberg Seatex as subcontractor. Space Norway is the design authority and owner of the VDE-SAT payload on-board the NorSat-TD satellite, which will be used as part of the project. This LEO-satellite was launched on April 15 2023 to about 500 km altitude, in a polar and sun-synchronous orbit with an inclination of 97.4°, and has an expected mission lifetime of three years[5]. This new technology demonstrator (TD) satellite gives Space Norway a unique opportunity to quickly test the concept of a VDE-SAT payload for demonstrative PNT-services without the need for new VDES infrastructure or changes to the ITU-approved VDES standard. In turn, the project provides an opportunity to answer the open questions on the effect of propagation effects, and verification of the performance of VDE-SAT as a PNT-source.

1.4. Research objective

The motivation behind the development of VDE-SAT pseudoranges is the apparent weaknesses in the Arctic region associated with the continued reliance on traditional GNSS. The successful launch of the NorSat-TD satellite has allowed for relevant VDES range measurements in the near-Arctic, which are obtained using a ground station located in Trondheim. This opportunity, its connection to the larger problem and the current knowledge gap, is summarised in the following research objective statement.

> To achieve a better understanding of the characteristics of empirical VDE-SAT ranging signals, and assess the current limitations and possibilities of VDE-SAT pseudorange acting as a source of PNT for critical navigation.

This is a top-level goal of the complete thesis project, which is further divided into three sub-goals. The first, and most central sub-goal for this research, is the one concerning the characteristics of the signal. Since the use of VDE-SAT ranging signals is an entirely new technology, an important aspect of the research is first to characterise the performance and behaviour of the signal. This is done by way of a statistical assessment of the ranging signal. The inherent statistical properties of the signal are evaluated using the available data, and the influence of the time-delay due to the ionosphere is investigated as a primary source of error in the signal. The second sub-goal ties directly to the main research question, and is one that questions the performance level possible for a semi-autonomous VDE-SAT PNT-service. This is an important question to answer, as the long-term goal is to obtain a PNT-service that does not rely on GNSS. The state-of-the-art research indicates that the novel VDE-SAT pseudoranges are too imprecise to replace GNSS entirely, but what may be possible in the future based on the contemporary empirical performance of the system has not yet been quantified. The third and final sub-goal assess the positioning performance of a combined system of VDE-SAT and GNSS PNT-sources. More directly applicable to the contemporary problem, the topic of the combination of GNSS and a VDE-SAT PNT-source will answer the question of current possibilities with the state-of-the-art VDES technology. The multiple source performance of a VDE-SAT PNT-source is therefore an important and contemporary topic following the main research question.

[4]URL https://navisp.esa.int/project/details/112/show, Accessed 6/10/2023.
[5]URL https://database.eohandbook.com/database/missionsummary.aspx?missionID=1012, Accessed 6/11/2023.

2
Journal Article

SPECIAL ISSUE PAPER

Characteristics of Experimental VDE-SAT Ranging Signals and System Performance Analysis for Critical Navigation

Øyvind Bryhn Pettersen[1]

[1]Faculty of Aerospace Engineering, TU Delft, Delft, the Netherlands

Correspondence
Øyvind Bryhn Pettersen, Space Norway AS, 0277 Oslo, Norway
Email: oyvind.pettersen@spacenorway.no

Present address
Space Norway AS, 0277 Oslo, Norway

Funding information
NAVISP, European Space Agency

Summary

Traditional Global Navigation Satellite Systems (GNSS) are subject to intentional or unintentional disturbances in the northern regions of Norway, leading to loss of critical infrastructure. The novel VHF Data Exchange System (VDES) has been suggested as an alternative positioning, navigation and timing (PNT) system for a possible GNSS-contingency service, based on signal simulations and statistical estimates. However, an empirical investigation into the feasibility of such a GNSS-contingency service remains to be done, and has only recently become possible after the launch of the NorSat-TD satellite with purpose-designed VDES ranging capabilities. This paper presents an analysis of the characteristics of empirical VDE-SAT range measurements and a system-level performance analysis of a GNSS-contingency system based on the signal performance of empirical ranging data gathered from NorSat-TD. Using the equated error level of the signal, the positioning performance of simulated autonomous systems of VDE-SAT PNT-sources is analysed, followed by an assessment of the combination of the empirical VDE-SAT range measurements and traditional GNSS measurements in a critical GNSS-contingency scenario. In total, 236 VDE-SAT pseudorange observations obtained from eleven satellite passes recorded in July 2023 were used. Residual analysis shows that these observations have a large and constant mean error of about 416 km, with a standard deviation of 260.8 m. The previously neglected atmospheric propagation effects on a VDE-SAT range measurement is shown to be significant, and the largest effect is likely to be the time-delay due to the ionosphere. The system performance analysis shows that VDE-SAT as a PNT-source could be used as a possible future general navigation backup system, with a positioning accuracy within 1000 m. Finally, an important conclusion is that a contemporary GNSS-contingency system is possible with the measured signal performance, where NorSat-TD acting as a PNT-source can, under the correct geometric conditions, allow a positioning accuracy within 1000 m in combination with partial GNSS coverage at the user.

1 | INTRODUCTION

Significant disturbance of Global Navigation Satellite System (GNSS) is affecting critical infrastructure in the northern regions of Norway, and the problem is becoming increasingly common the past years[1 2 3]. Alternative navigation systems are needed to ensure continued operations under critical GNSS-down conditions, driving the development of purpose-designed ranging signals using alternative communication systems. The topic of this paper is the analysis of experimental pseudorange measurements over the novel VHF (very high frequency) Data Exchange System (VDES) acting as a source of position, navigation and timing (PNT) information in regions known for poor GNSS coverage.

[1]URL `https://www.nrk.no/tromsogfinnmark/kraftig-okning-av-gps-jamming-over-finnmark-1.16309499`, Accessed 03/10/2023.
[2]URL `https://www.nrk.no/tromsogfinnmark/mangedobling-av-gps-jamming-mot-norge-1.16563000`, Accessed 03/10/2023.
[3]URL `https://www.tv2.no/nyheter/innenriks/ambulansefly-kunne-ikke-lande-etter-gps-utfall/10397144/`, Accessed 03/10/2023.

VDES is an evolution of the well-establish Automatic Identification System (AIS), which was first investigated as a source of alternative ranging signals in the project ACCSEAS (Johnson and Swaszek, 2014). Further research on the topic saw VDES in ranging mode (R-mode) outperforming that of AIS, shifting the focus to the digital exchange system (Šafář et al., 2020). The current state-of-the-art research has resulted in statistical lower bounds of the performance of the satellite component of VDES, namely VDE-SAT, based on simulation studies, and experimental results only of the terrestrial VDES component, VDE-TER (Šafář et al., 2021; Wirsing et al., 2023). An important novelty of this research is then the analysis of the ranging performance of experimental VDE-SAT range measurements. This study is also expanded to compare studies of simulated constellations of VDE-SAT capable satellites acting as augmentation or backup to GNSS, with the system performance of the same constellations providing range measurements with signal performance equal to that of the empirical data (Šafář et al., 2018; Owens et al., 2021).

This work is made possible in support of European Space Agency (ESA) project ICING, funded by the Navigation, Innovation and Support Program (NAVISP) of ESA, lead by Space Norway out of Oslo, Norway, with subcontractor Kongsberg Seatex in Trondheim, Norway. Space Norway is the design authority and owner of a VDE-SAT payload on-board the NorSat-TD satellite, which will be used as part of this project. This gives a unique opportunity to gather empirical data to test the concept of using a VDE-SAT payload for demonstrative PNT-services. The objective of this study is to achieve a better understanding of the characteristics of VDE-SAT ranging signals, and assess the current limitations and possibilities of VDE-SAT pseudorange signals acting as a PNT-source for critical navigation. This is done by means of a statistical parametric analysis of empirical pseudorange measurements, and a system performance analysis by way of simulating the identified signal characteristics in select system variations.

The paper begins by describing the details of the gathered empirical data, in section 2. This section describes the testing infrastructure, the range measurements and required auxiliary data, and provides an overview of the data set that serves as input to the analysis. Further, section 3 describes the applied methodology, starting with the method used to describe the signal characteristics in section 3.1. There, the basic statistical and parametric analyses are described, as well as the applied signal corrections. The last section of the methodology is section 3.2, which details the methods used to evaluate the system performance, using the signal characteristics identified in the previous section. All results are shown in section 4, and further discussed in section 5. The paper ends with conclusions and recommendations for further work in section 6.

2 | DATA DESCRIPTION

The topic of analysis for this research paper are the first empirical VDE-SAT range measurements. This section will first present the surrounding infrastructure used for the testing campaign, where the information is largely based on internal project design and interface documents. Further, the section will present the information from the observation-, navigation- and telemetry-data that is used for the analysis. Finally, the section concludes by presenting the resulting measurements from the test campaign that will be used in the analysis of this paper.

2.1 | Testing infrastructure

All VDE-SAT data is gathered through the same link, which is a one-way link from the NorSat-TD satellite to a dedicated ground station located in Trondheim, Norway. NorSat-TD was launched on April 15 2023 into a low-Earth orbit (LEO), at an approximately 550 km altitude. On-board the satellite is a VST x50 VDES transceiver produced by Kongsberg Seatex and owned by Space Norway, connected to a 3-element 8 dBi Yagi-Uda antenna in an Earth-limb pointing mode, transmitting signals at a 161.8625 MHz frequency. A modified firmware of the VST x50 transceiver is required for the ranging capabilities needed for this project, but the transmitted signals are physical layer-compatible with the defined specification of VDES Link ID 29 with a 150 kHz bandwidth (ITU-R, 2022). The VDES transceiver receives its required pulse-per-second (PPS) input directly from a GNSS receiver on-board the satellite, meaning a key assumption for this project is that the satellite remains time-synchronized to GNSS through a valid PPS input.

The ground terminal consists of a VDE terminal, an external clock source, and the receiving antenna. The VDE terminal is a modified Kongsberg Seatex VDES 300 ship-terminal, with a GNSS and VHF antenna interface. This terminal uses a μBlox GNSS timing module, and an external high precision Kongsberg 10 MHz rubidium clock as a timing source. The VHF antenna is a dipole Comrod AV7M antenna, designed for maritime communication, and seen at the top of the array in Figure 1. The location of the antenna is given in Table 1, in geodetic coordinates and the WGS84[4] earth-centred, earth-fixed (ECEF) reference frame.

FIGURE 1 The ground station antenna mounted at the top of the array, on the roof of Pirsenteret in Trondheim, Norway.

TABLE 1 The position parameters of the ground station antenna.

Pos. element	Value
Latitude	63.441518°
Longitude	10.403556°
Height	37.0 m
X_{ECEF}	2812.412 km
Y_{ECEF}	516.355 km
Z_{ECEF}	5682.185 km

[4]URL `https://earth-info.nga.mil/?dir=wgs84&action=wgs84`, Accessed 6/10/2023.

2.2 | Measurements and auxiliary data

The ranging measurements included in this work were recorded on three days, July 11th, 18th and the 25th, for all satellite passes on these days. The measurements were sorted by pass, and distributed in three distinct parts. First, the observation measurements provide the results at the receiver, which include the VDES slot number S_n of the measured ranging burst, time offset Δt, and information on the signal quality with a measure of the signal-to-noise ratio (SNR). These measurements also contain an error check using cyclic redundancy check (CRC), to detect packet losses in the received message (Sheng-Ju, 2015). An observation set O is given in Equation 1. Secondly, in the event of no packet loss, the transmitted navigational message N is also recorded at the receiver. This contains the proprietary navigational message as defined at the time of transmission, with satellite position $\mathbf{r_t}$ and velocity $\mathbf{v_t}$ in the WGS84 ECEF-frame and timestamp of transmission t_t in Coordinated Universal Time (UTC), summarised in the set in Equation 2. Finally, auxiliary NorSat-TD telemetry data was used in the analysis. Included in the set T of telemetry data in Equation 3 is an alternative satellite position $\mathbf{r_t^{TEL}}$ and velocity $\mathbf{v_t^{TEL}}$, given in the same ECEF-frame and evaluated at the time of transmission t_t.

$$O = \{S_n,\ \Delta t,\ \text{SNR},\ \text{CRC}\} \tag{1}$$

$$N = \{t_t,\ \mathbf{r_t},\ \mathbf{v_t}\} \tag{2}$$

$$T = \{\mathbf{r_t^{TEL}},\ \mathbf{v_t^{TEL}}\} \tag{3}$$

A pseudorange measurement is a simple range measurement based on the time-of-flight of a transmitted signal (Milliken and Zoller, 1978). In the VDES one-way link described in section 2.1, both the transmitter and receiver slot timing is synchronized to UTC time through a GNSS PPS signal. The time offset at the ground station between the start of the slot S_N, also reported as the timestamp t_t at which the ranging signal was transmitted, to the time at the receiver t_r is measured using proprietary time estimation techniques, as a measure of the time-of-flight of the signal, meaning $\Delta t = (t_r - t_t)$. Each measurement of the time offset can then readily be transformed into a pseudorange measurement at the time of reception by multiplying the time difference by the speed of light in a vacuum, as seen in Equation 4.

$$\tilde{\rho}(t_r) = c \times (t_r - t_t) \tag{4}$$

The ranging signals are made possible by modifications to the ranging burst transmitted over the VDE-SAT downlink SAT-MCS-0.150 (Link ID 29) format (IALA, 2019). Simulations of the physical layer of this ranging burst, conducted by Kongsberg Seatex, show that the timing estimate error in Δt, neglecting all other noise-contributing effects, introduces a standard deviation of 274.8 ns in each pseudorange $\tilde{\rho}$, or equivalently 82.2 m. The simulations are conducted with a realistic carrier-energy-to-noise-ratio $E_c/N_0 = -13.5$ dB, which with the implemented spreading factor of 2 is approximately equivalent to an SNR of $E_s/N_0 = -10.5$ dB. Little improvement is seen in the timing estimate error with increasing SNR. This can then be considered a lower bound of the possible range error with the modified ranging burst. This lower estimate is based on simulations entirely neglecting propagation effects, meaning it is a performance bound for ranging signal propagation error corrections. The quantified timing error corresponds well with literature on the performance bound of VDES ranging signals (Šafář et al., 2020, 2021). The introduced bias from the transmitter is not known in detail, and is expected to be measured and introduced as part of the navigational set N in later iterations

The reported satellite position in the transmitted navigational message N could not be used in the analysis, as the satellite firmware did not have full functionality during the test campaign, missing this feature. The recorded satellite telemetry in the set T was implemented to be used in the analysis, as an alternative source of the satellite position. This recorded satellite telemetry comes from the same GNSS receiver that transmits the required PPS input to the VDE-SAT payload. The telemetry is recorded in minute-intervals, and the satellite position was interpolated between these intervals using a cubic spline interpolation with a "not-a-knot" boundary condition at either end, to the timestamp of transmission t_t. The first derivative of the cubic spline was used as the satellite velocity. The faulty navigational message entries of N were in that way circumvented by using the satellite telemetry in T as an alternative.

The results of the test campaign in the month of July resulted in eleven passes across three days, shown with key data metrics in Table 2. In total, 242 pseudorange observations were measured with no packet loss. Additionally, the principle of studentized residuals are applied, where measurements of a pass that deviate past three standard deviations away from the mean of that pass are assumed outliers (Thompson, 1935). Eliminating measurements three standard deviations away from the mean correspond approximately to eliminating the 95th-percentile of a sample size between 30 and 40, which is a typical sample size for a single pass (Tietjen et al., 1973). Further, a few measurements were manually identified as outliers. In total, six observations were identified as outliers in pass 18/7 - 4, and 25/7 - 3, as large discrepancies from the other range measurements of the same pass, making the total number of observations included in the analysis 236 pseudorange observations. The resulting final set A is seen in Equation 5 as combination of the elements of O, N and T, with the timestamp, time offset and signal quality metric, satellite position and velocity as sourced from the telemetry. This is all the information needed at each observation to complete the analysis.

TABLE 2 An overview of the passes included in the analysis with summarising information on the data. The listed timestamps are those of the first observation of each pass, each indicating the time since January 1, 2000, at 12:00 UTC time.

Identifier	Timestamp [s]	# of obs.	Outliers
11/7 - 1	742307112.0	31	-
11/7 - 2	742323770.4	12	-
11/7 - 3	742334750.4	47	-
18/7 - 1	742914271.2	31	-
18/7 - 2	742919884.8	4	-
18/7 - 3	742930872.0	11	-
18/7 - 4	742936411.2	27	Last 4
18/7 - 5	742941904.8	37	-
25/7 - 1	743521363.2	15	-
25/7 - 2	743526991.2	3	-
25/7 - 3	743554744.8	18	Last 2
Total	-	**236**	**6**

$$A = \{t_t,\ \tilde{\rho}(t_r),\ \text{SNR},\ \text{CRC},\ \mathbf{r}_\mathbf{t}^{\text{TEL}},\ \mathbf{v}_\mathbf{t}^{\text{TEL}}\} \tag{5}$$

3 | METHODOLOGY

The research is separated in two parts. First, the signal characteristics are evaluated by means of a statistical analysis of the residual of the empirical range measurements. The method used for this analysis is described in section 3.1. Secondly, based on the signal characteristics evaluated in the first part, the positioning performance of various simulated VDE-SAT systems is analysed, as well as the empirical single satellite positioning performance. The methodology of this analysis is presented in section 3.2.

3.1 | Signal characteristics

The analysis of empirical VDE-SAT signals is a central part of the novelty of this work. The key characteristics of this novel ranging signal is first investigated using fundamental descriptive statistics of the evaluated pseudorange residuals. Following is a more thorough parametric analysis, and finally a study of the applicability of established GNSS signal correction techniques to the measured pseudoranges.

Each pseudorange measurement is defined as in Equation 6, with a relation to the true geometric range ρ_{true}, the speed of light c, equal to 299792458 $\text{m}\,\text{s}^{-1}$, and relative time offset between transmitter and receiver clock $\delta t = \delta t_r - \delta t_t$, and finally an error term $\delta\rho_\epsilon$, comprising of all error sources in the propagated signal (Milliken and Zoller, 1978). Because all pseudorange measurements are fundamentally a measurement of the time-of-flight of an electromagnetic wave, the term $\delta\rho_\epsilon$ will include any effect on a propagating electromagnetic wave. The most notable effects considered in GNSS are the individual receiver and transmitter clock errors, observation noise, ephemeris errors, multipath, and atmospheric delays. Simple models of different error effects on VDES ranging signals have shown that it is the atmospheric effects, and in particular the time-delay due to the ionosphere, that is the most important effect (Owens et al., 2021). In this regard, only the time-delay due to the ionosphere will be considered in the error term $\delta\rho_\epsilon$ in this analysis.

$$\tilde{\rho}(t_r) = \rho_{\text{true}} + c \times \delta t + \delta\rho_\epsilon \tag{6}$$

3.1.1 | Residual pseudorange analysis

To assess the quality of the VDES range observations, residual measurements are derived by comparing the pseudorange measurement with the computed true range. These residuals are statistically analysed as a first assessment of the signal characteristics. This section will detail the processing of the pseudorange residual measurements, and the method used to find the fundamental statistical properties of this dataset.

Let the NorSat-TD telemtry position $\mathbf{r}_\mathbf{t}^{\text{TEL}}$ and velocity $\mathbf{v}_\mathbf{t}^{\text{TEL}}$ be simply denoted as $\mathbf{r}_\mathbf{t}$ and $\mathbf{v}_\mathbf{t}$, respectively. The pseudorange residuals e_ρ are defined as the difference between the measured VDES pseudoranges $\tilde{\rho}$ and the geometric range between the transmitting NorSat-TD position $\mathbf{r}_\mathbf{t}$ and the receiving ground station antenna position $\mathbf{r_r}$, as seen in Equation 7. In reality, both $\mathbf{r_t}$ and $\mathbf{r_r}$ are estimates. As described in section 2, the position of the ground station and satellite are accurately known, and it is assumed that $e_\rho >> \epsilon_r$, the error in the geometric range estimate.

$$e_\rho = \tilde{\rho}(t_r) - |\mathbf{r_r}(t_r) - \mathbf{r_t}(t_t)| \tag{7}$$

Each constructed residual e_ρ can be considered an independent random variable for the further statistical analysis. As presented in section 2, each measurement consists of a pseudorange measurement and an associated navigational message containing the transmitted auxiliary data. When the ground position is known, each measurement contains the information needed to form precisely one residual. Assuming each measurement can be considered independent, the same can be inferred for the pseudorange residuals evaluated using Equation 7. In this case, the residual measurement can be seen as an independent continuous random variable, and it is of interest to evaluate the statistical spread and bias, as well as a probability density function associated with this random variable.

The distribution of the pseudorange residuals listed in Table 2 was then analysed. The descriptive statistics of the dataset was calculated: its mean, variance, skewness and kurtosis. This was applied to each satellite pass individually, as well as the total set of all observations. The residual measurements were then fit to a collection of continuous probability distributions. The four chosen distributions were the *normal*, *skew-normal*, *log-normal* and *Rice* distributions. The normal distribution is considered because the equivalent error in a GNSS pseudorange measurement is often assumed normally distributed, although this is known to overbound the true error (DeCleene, 2000). The skew- and log-normal distributions were chosen for their varying skew and tail properties, based on the assumed normal distribution (O'Hagan and Leonard, 1976). Further, experience with VDE-SAT transmission at Space Norway has shown that the measured signal-to-noise ratio follow a Rician distribution, which is also included as one of the analysed distributions.

To compare the relative fit of the four distributions, the Kolmogorov-Smirnov (KS) test is employed to evaluate the probability that the residual measurements follow the given distribution (Shiryayev, 1992). The KS-test, which evaluates the distance between an empirical distribution and a cumulative distribution function, is known to be a poor test for normality in an empirical distribution where the mean and variance are both unknown and instead must be calculated from the data, as is done in this methodology (Stephens, 1974). In that regard, this test was only employed as a relative measure of fit between the four distributions. In addition, the Anderson-Darling (AD) test, which is shown in Stephens (1974) to be a better test for normality than the KS-test, is used to evaluate the fit of the normal distribution for a more definite conclusion on the goodness-of-fit (Anderson and Darling, 1952).

3.1.2 | Parametric analysis

To identify the performance characteristics of the pseudorange measurements more thoroughly, a parametric analysis was applied, where the statistical behaviour of the pseudorange residuals was estimated using a given set of input parameters. By comparing the computed pseudorange residuals to a variety of external parameters, our understanding of the data can improve, and the characteristics of the signal could be explained by the influence of the chosen parameters. This analysis resulted in a more complete evaluation of the signal characteristics.

The method of parametric analysis is a simple and multiple linear regression. By assuming a linear relationship between a response Y and a single predictor X, the relationship can be represented as in Equation 8, showing the approximation of the response using the defined and constant model parameters β_0 and β_1 (James et al., 2013). These coefficients are unknown, and are estimated as $\hat{\beta}_0$ and $\hat{\beta}_1$ using observations. A dataset of n observations of the response and predictor can be expressed as the set of n amount of pairs $(x_1, y_1),\ (x_2, y_2),\ \dots,\ (x_n, y_n)$. The estimated response, using the model coefficients, is then $\hat{y}_i = \hat{\beta}_0 + \hat{\beta}_1 x_i$ for $i = 1, \dots, n$. Using the least-squares method, the coefficient estimates $\hat{\beta}_0$ and $\hat{\beta}_1$ are chosen such that the residual sum of squares $\text{RSS} = \sum_{i=1}^{n}(y_i - \hat{y}_i)^2$ is minimized.

$$Y \approx \beta_0 + \beta_1 X \tag{8}$$

The pseudorange residuals were also modelled using multiple predictors in a multiple linear regression. A number of predictors $X_1, X_2, \dots, X_p$ and defined and constant model coefficients $\beta_0, \beta_1, \dots, \beta_p$ were used to approximately model this linear relationship, as seen in Equation 9. As for the simple linear regression, the coefficients were estimated by applying the least-squares method to minimize the RSS.

$$Y \approx \beta_0 + \beta_1 X_1 + \cdots + \beta_p X_p \tag{9}$$

The set of parameters that are included in the analysis are the four parameters that are hypothesised to be most influential. The first considered parameter is the SNR. For conventional GNSS signals, the SNR has been shown to be strongly correlated with the experienced multipath errors, and correction methods exist where the multipath delay is modelled as a direct function of SNR (Breivik et al., 1997). The other three parameters relate to the ionospheric time-delay, as this has been highlighted as a critical error source for the relatively low-frequency, and therefore dispersive, VDES ranging signals (Owens et al., 2021). These parameters are the pseudorange measurement $\tilde{\rho}(t_r)$, computed elevation angle of the satellite, and time-of-day of the timestamp t_t. The first two are related to the geometric range through which the ionospheric delay accumulates. The time-of-day is included to display an expected variation in local ionosphere electron content, a quantity that is directly related to the ionospheric time-delay (Klobuchar, 1987). The time-of-day was not included in the linear regression analysis, as the expected correlation between the ionospheric time-delay and the time-of-day is a half-cosine, not linear (Klobuchar, 1987). Additionally, the measured pseudorange has been shown to be correlated with increasing error in terrestrial VDES ranging experiments (Wirsing et al., 2019). The four parameters SNR, pseudorange, elevation angle and time-of-day are expected to be the most influential, and were therefore included in the parametric study. Each parameter was normalized to a range $[0, 1]$, where 0 correspond to the lowest measured value of the parameter, and 1 the highest.

The individual parameter contributions were evaluated using the standard error and t-statistic associated with the estimated coefficient. As each model coefficient is an estimate of the assumed approximate linear relationship in Equation 9, the computed value comes with an inherent variance. Assuming the error of each observation is uncorrelated to all other observations, and that they share a common variance σ^2, the standard error (SE) of one parameter describes this inherent variance of the coefficient value as a result of the sample error and its variance σ^2.

From the standard error follows the definition of the t-statistic and its associated p-value that is central in this analysis. Fundamentally, the t-statistic evaluates if a computed coefficient is sufficiently far from zero to be assumed non-zero, given the computed standard error of the coefficient. It is computed as seen in Equation 10. Conversely, assuming the parameter $\beta_i = 0$, a measure of the probability that any number is larger than $|t|$, for the normally distributed t-statistic, gives an equivalent measure that is more directly interpretable as the probability that the computed coefficient is, in fact, zero. This measure is called the p-value, evaluating the probability of observing a number larger than $|t|$ assuming the coefficient is zero, and a typical threshold value of 5% is used to confirm that a computed coefficient is non-zero, and therefore has a significant relationship with the pseudorange residuals.

$$t = \frac{\hat{\beta}_i - 0}{\mathrm{SE}(\hat{\beta}_i)} \tag{10}$$

When evaluating the fit of the whole regression model, the well-known R^2-metric was used. This is a relative metric, in the range $[0,\ 1]$, describing the proportion of total variance in the response Y that can be explained by the predictors X in the regression (James et al., 2013). In systems where a linear model is only a rough estimation of the behaviour of Y, as is the case for this non-linear system, the R^2-metric may return values well below 0.1. It is used in this analysis only as a relative measure of fit between the different regression models.

3.1.3 | Ionospheric signal corrections

It is hypothesised that the dominant contribution to the pseudorange error is the time-delay due to the ionosphere. It is therefore of interest to evaluate the applicability of established GNSS atmospheric correction techniques to VDE-SAT pseudorange measurements. Three different correction models were applied: The Klobuchar and the NeQuick-G model, primarily applied to the GPS and Galileo navigation systems, respectively, and a global ionosphere map published by the International GNSS Service (IGS).

The ionospheric corrections implemented in the GPS broadcast ephemeris use a simple and easily applicable algorithm based on the work presented by Klobuchar (1987), and is colloquially called the Klobuchar model. The algorithm captures "the main features of the complex behaviour of the ionosphere" (Klobuchar, 1987, p. 325), with a focus on a computationally efficient algorithm that reduces the effect of the ionosphere on the measured range by 50%. The algorithm implements a day-time variation in time delay, in the shape of a half-cosine, with coefficients to vary the amplitude and period of the correction. There is no night-time variation in the time-delay, and the model assumes the total influence of the ionosphere to act in a shell at 350 km altitude, with no consideration for variation in height at the transmitter. The model is based on a function of frequency, and is therefore directly scalable to VDES frequencies by an inverse-square relationship.

The ionospheric model used for single-frequency time-delay corrections in the European Galileo satellite navigation system is called NeQuick-G (European Commission, 2016), derived from the NeQuick electron density model, and adapted to an algorithmic form for the application in Galileo. This model incorporates the influence of height variation in the electron density and the height of the transmitter, in contrast to the Klobuchar model. The output of the model is the Slant Total Electron Count (STEC), which when combined in Equation 11 with the frequency of the transmitted signal, equate to a measure of the ionospheric group delay $d_{\mathrm{I}gr}$, which was applied as a time-delay correction of the associated pseudorange measurement $\tilde{\rho}(t_r)$. Because this delay is a function of the frequency, this model becomes directly applicable to VDES pseudoranges, although the model has not been validated at VHF frequencies.

$$d_{\mathrm{I}gr} = \frac{40.3}{f^2} \cdot \mathrm{STEC} \tag{11}$$

The final correction model that was applied was the IGS Global Ionosphere Map (GIM). While the Klobuchar and NeQuick-G models are designed for real-time assessment of ionospheric time-delay, there are also options for offline post-processing models. When using these models, it is not possible to perform a real-time correction, but a more accurate description of the ionosphere can be acquired for the analysis. IGS uses data from eight analysis centres and over 400 GNSS stations to form a vertical total electron content (TEC) map, published to the public domain[5]. The map is a grid given in latitude and longitude, and over time, typically in a 15-minute temporal resolution, and was linearly interpolated in both positional

[5]URL `https://igs.org/wg/ionosphere/`, Accessed 20/9/23.

and temporal directions. The given values for the total vertical electron content are assumed in a single layer at a set altitude, typically called a thin shell model. By calculating the ionospheric pierce point at the given altitude of the thin shell, in a straight line between the transmitter and receiver, the local vertical TEC at the pierce point was evaluated. This was then mapped to a slant TEC along the line-of-sight using a modified single-layer model mapping function (Grejner-Brzezinska et al., 2004, Eq. 5). This was translated to a time-delay due to the ionosphere using the function for the ionospheric group delay that was used for the NeQuick-G model, given in Equation 11.

Each correction model was applied to each VDE-SAT pseudorange measurement, and the total set of corrected residuals were analysed and compared using the methods of section 3.1.1 and section 3.1.2.

3.2 | Positioning performance analysis method

The analysis of the positioning performance of a VDE-SAT PNT-source acting in a navigation system is divided in three parts. First, the employed positioning algorithm is described. Secondly, the positioning performance of VDE-SAT ranging signals acting autonomously, with no other sources, is evaluated. This is divided in an analysis of the single-satellite positioning performance, and simulated systems of constellations of VDE-SAT PNT-sources. Thirdly, the positioning performance of these same ranging signals acting in a multi-source system with GPS is evaluated. The topic of this section will be the combination of VDE-SAT with GNSS for an evaluation of the current capabilities of VDE-SAT ranging signals as a contingency system. The positioning performance analysis is limited by the assumptions of a GNSS-disciplined clock and satellite position.

3.2.1 | Positioning algorithm

The analysis of positioning performance requires a positioning algorithm for combining multiple range measurements into a positioning solution. This section will present the implemented algorithm used for all positioning evaluations further in the positioning performance method.

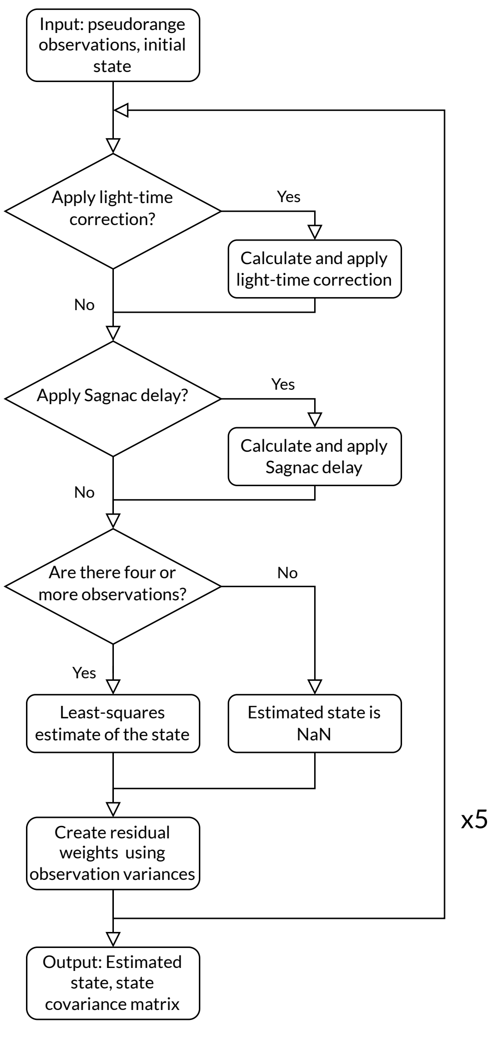

FIGURE 2 A flow diagram of the positioning algorithm, highlighting the order of corrections and iteration.

One of the most fundamental methods of determining the receiver position is through the use of a linearised and iterated least-squares estimate. Let $\tilde{\rho}$ denote the $n \geq 4$ pseudorange observations of the positioning problem, and let ρ denote the computed pseudorange between the transmitter and the estimated state $\mathbf{x} = [x_r,\ y_r,\ z_r,\ c \cdot \delta t]^T$, as seen in Equation 12. The least-squares problem can then be formulated as in Equation 13 as a function of the estimated state vector $\mathbf{x}$. This problem is solved using the Levenberg-Marquardt algorithm, a numerically robust method well-suited for collinear problems (Moré, 1978).

$$\rho(\mathbf{x}) = \sqrt{(x_t - x_r)^2 + (y_t - y_r)^2 + (z_t - z_r)^2} + c \cdot \delta t \tag{12}$$

$$\Phi(\mathbf{x}) = \sum_{i=1}^{n} f_i^2(\mathbf{x}) = \sum_{i=1}^{n} (\tilde{\rho}_i - \rho(\mathbf{x})_i)^2 \tag{13}$$

The problem design matrix, $\mathbf{H}$, is an $n \times m$ matrix defined following a first-order Taylor expansion of Equation 12. Its elements are the negative partial derivatives of each element of the state $\mathbf{x}$. It was calculated as the negative Jacobian matrix, $\mathbf{J}$, where the element (i, j) correspond to the partial derivative $\partial \rho_i / \partial x_j$ of the pseudorange ρ in Equation 12 with respect to the state element x_j.

The algorithm is applied five times for each positioning problem, applying up to two corrections between iterations. If the measurement and satellite position are both sampled at the time at the receiver t_r, a light-time correction of the satellite position is required. This is to compensate for the satellite travel during the signal time-of-flight. Because this is not the case for all inputs to the algorithm, the correction is parametrized as a property of each observation. The corrected satellite position $\mathbf{r}_t^*$ is calculated as a linear change in position using the instantaneous velocity of the satellite, as seen in Equation 14 with $|\mathbf{r}_t - \hat{\mathbf{r}}_r|$ denoting the absolute distance between the satellite and the estimated position. In case the satellite position is given in an ECEF-frame, another correction must be applied. Due to the rotation of the Earth, the ECEF reference frame, $\mathbf{E}$, rotates between the time at signal transmission and reception. The satellite position vector $\mathbf{r}_t$, defined at the time of transmission t_t in the reference frame $\mathbf{E}_t$, is therefore distinct from the same vector at the time of reception, t_r, in reference frame $\mathbf{E}_r$. Let the receiver position $\mathbf{r}_r^{\mathbf{E}_r} = [a, b, d]^T$

and the satellite position $\mathbf{r}_t^{\mathbf{E}_t} = [x, y, z]^T$, then the error in each pseudorange measurement ρ due to the rotation of the ECEF frame, called the Sagnac delay, was corrected using the expression in Equation 15, to find the corrected range ρ^*, with the Earth angular rotation rate ω_e, equal to 7.292115×10^{-5} rad s^{-1} (Hu and Farrell, 2019). These corrections ere applied only where necessary, which varies depending on the source of the data used in the positioning problem. An illustration of the iteration of the positioning solution can be seen in Figure 2.

$$\mathbf{r_t}^* = \mathbf{r_t} - \frac{|\mathbf{r_t} - \hat{\mathbf{r}}_r|}{c}\mathbf{v_t} \tag{14}$$

$$\rho^* = \rho + \frac{\omega_e}{c}(xb - ay) \tag{15}$$

If the measurement variance is known, the position covariance matrix can be calculated, and the least-squares problem can be expanded to one of weighted residuals. The position covariance matrix is readily computed using the design matrix, $\mathbf{H}$, and the observation covariance matrix, $\mathrm{Cov}(\rho)$, the latter of which is defined as a diagonal matrix with entry (i, i) equal to the variance of observation ρ_i. The position covariance matrix is computed as in Equation 16 (Kaplan and Hegarty, 2006, Eq. 7.38). The inverse of the diagonal entries of the observation covariance matrix was applied as weights to the computed residuals, f_i, in the sum of the least-squares problem in Equation 13.

$$\mathrm{Cov}(\mathbf{x}) = (\mathbf{H}^T\mathbf{H})^{-1}\mathbf{H}^T\mathrm{Cov}(\rho)\mathbf{H}(\mathbf{H}^T\mathbf{H})^{-1} \tag{16}$$

3.2.2 | Autonomous positioning performance

To evaluate the opportunities of an autonomous VDE-SAT navigation system, the performance of the signal was put in the context of different autonomous systems of VDE-SAT PNT-sources. To consistently compare the results of different systems, a common error metric was established. The positioning accuracy of a system was defined as a surface position error, computed as the great-circle distance over the WGS84 geoid. This was computed using the Haversine formula, a computationally efficient trigonometric relationship that is also numerically stable for small distances (Bullock, 2007).

First, the current performance potential of the system was evaluated using only the empirical range measurements. This was done using a rolling positioning accuracy measure, where N consecutive measurements of a total of n in a particular pass was used to calculate the position of the ground station antenna over time through that particular pass. As the satellite positions are reported in an ECEF-frame, a Sagnac delay correction was applied to the measured pseudoranges. The analysis was done for all integer N where $4 \le N \le n$ for all passes. The mean surface position error through each pass for a given N was calculated. The analysis was repeated with an additional surface constraint. This was done to emulate the performance of a more sophisticated geoid-constrained positioning solution, which is more applicable for ships in a maritime environment. The constraint was implemented as an additional pseudorange observation from the center of the Earth, with range equal to the norm of the true receiver position in an ECEF frame, with a 1m variance.

Further, to evaluate the possible positioning accuracy with the current ranging capabilities of VDE-SAT, different constellations of satellites were simulated and analysed. The two simulated constellations are selected from the recent feasibility study of VDE-SAT ranging in Owens et al. (2021), namely the Iridium NEXT and OneWeb constellations. Details of the simulated orbits are given in Table 3, taking note that the number of satellites in the Iridium constellation differs to that of Owens et al. (2021, Tab. 8) which has six more satellites. All satellites are assumed in an unperturbed Keplerian orbit, at an altitude of 550 km, different to that of Owens et al. (2021) which simulates the orbits at 600 km altitude, but closer to the planned altitude of the NorSat-TD satellite. Illustrations of the two simulated constellations can be seen in Figure 3. These two constellations were simulated over 24 hours, with a four minute time-step. At each timestamp, pseudorange observations with an inherent noise level equal to that obtained with the method explained in section 3.1.1 was gathered from all satellites visible above the horizon. All satellite positions were evaluated at the time of reception of the signal t_r, meaning a light-time correction was necessary to find the satellite position at the time of transmission t_t. The measurements were simulated in an inertial frame, meaning no Sagnac delay correction was necessary.

TABLE 3 Details of the VDE-SAT constellations included in the autonomous performance analysis.

Constellations	Orbital planes	Inclination	Satellites per plane	Total number of satellites
Iridium NEXT	6	86.5°	11	66
OneWeb	12	86.4°	54	648

A positioning performance metric and geometric performance metric were computed and compared to the results of Owens et al. (2021). A positioning solution was computed at each timestamp, and a surface position error was defined as the difference over the geoid-surface between this computed position and the known true position of the antenna, calculated using the spherical law of cosines. Additionally, the geometric distribution

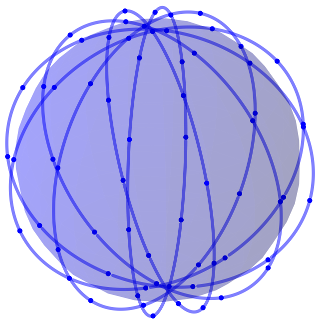

(a) The simulated Iridium NEXT constellation.

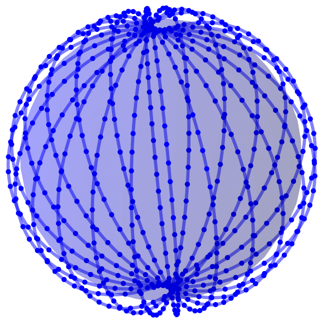

(b) The simulated OneWeb constellation.

FIGURE 3 Illustration of the two simulated constellations around a transparent globe.

of satellites was evaluated by computing the dilution of precision (DOP), in particular the local horizontal DOP (HDOP). Using the design matrix $\mathbf{H}$ to evaluate the matrix $\mathbf{K} = (\mathbf{H}^T\mathbf{H})^{-1}$, which is a function only of geometry, the elements of the diagonal in $\mathbf{K}$ describe the dilution of precision of the elements of the state vector. By rotating the matrix $\mathbf{K}$ to $\mathbf{K}^{\text{ENU}} = \mathbf{RKR}^T$, with the rotation matrix $\mathbf{R}$ describing the rotation from ECEF to the local East-North-Up (ENU) frame, the local horizontal DOP can be evaluated as in Equation 17, with D_{11} and D_{22} the first and second element of the diagonal in $\mathbf{K}^{\text{ENU}}$.

$$\text{HDOP} = \sqrt{D_{11} + D_{22}} \tag{17}$$

3.2.3 | Performance as backup service

An important contemporary application of VDE-SAT in a navigation system, is the combination of VDE-SAT range measurements with partial GNSS coverage. This was analysed by combining three GPS pseudorange observations with one empirical NorSat-TD pseudorange measurement, and calculating a surface position error of the resulting multi-source positioning solution. This error is directly compared to the posed minimum requirements for a maritime navigation backup system, as seen in Table 4 (IALA, 2012). These requirements are posed by the International Association of Marine Aids to Navigation and Lighthouse Authorities (IALA) as a minimum performance level for a system that "ensures continuation of the navigation application, but not necessarily with the full functionality of the primary system" (IALA, 2012, p. 9). Ranging from AIS R-mode is listed as a planned terrestrial backup system with minimum performance standards, so the same standards were applied in this work to VDE-SAT ranging. The issues of GNSS-dependence in AIS is mentioned in IALA (2012), but are considered here as parallel challenges to the ranging performance of the system and are therefore not investigated in this work.

TABLE 4 The suggested minimum requirements for a general navigation-backup system, as presented in IALA recommendation R0129 (IALA, 2012, Tab. 2).

Environment	Absolute accuracy [m]
Ocean	1000
Coastal	100
Port approach and restricted waters	10
Port	1
Inland waterways	10

All GPS pseudorange observations were simulated by constructing a perfect geometric range between the receiver and a transmitting GPS satellite, with added noise and bias. Because the empirical GPS positions and range observations were evaluated at the same time, meaning $t_r = t_t$, no light-time or Sagnac delay correction was necessary for the GPS observations. The noise added to each measurement was a Gaussian noise with 4m standard deviation, approximately equivalent to the reported 7.8m 95% confidence interval of a single-frequency GPS range measurement (Montenbruck et al., 2018). The added relative time offset δt to the GPS range measurements is equal to that measured from NorSat-TD, resulting from the method in section 3.1.1, to allow the use of a single estimated time offset in the positioning algorithm. As the VDE-SAT satellite positions are reported in an ECEF-frame, a Sagnac delay correction was applied to the VDE-SAT pseudoranges. GPS positions were sampled from daily orbit solutions constructed and submitted by IGS (Griffiths, 2019). The final orbit solutions product is published typically 12-18 days after the day at hand, with a 2 cm accuracy,

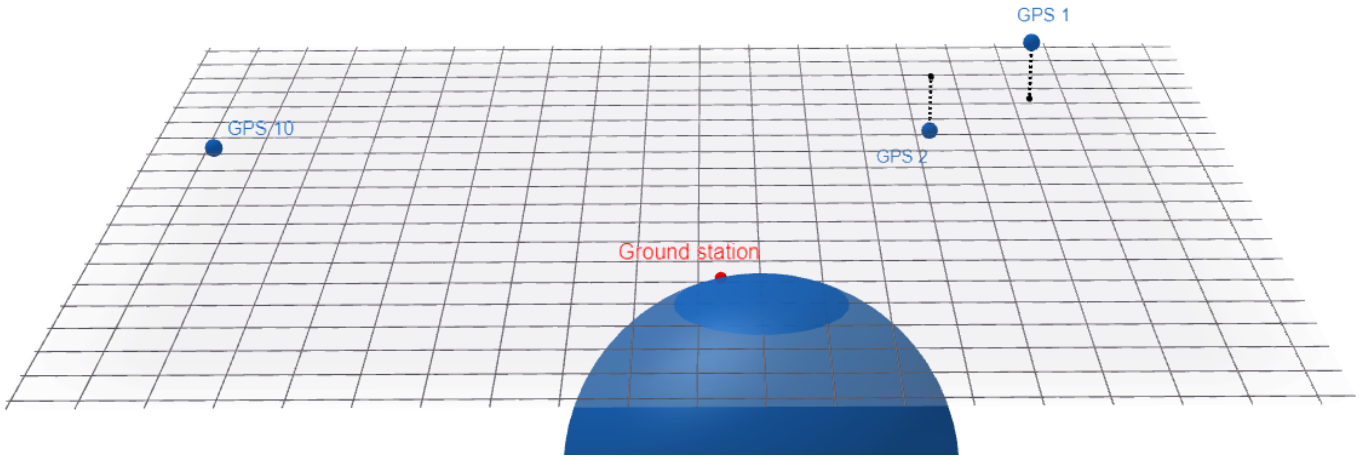

FIGURE 4 Three GPS satellites approximately in-plane with the ground station, making positioning impractical due to rank deficiency in the design matrix.

and a sample frequency of 15 minutes (Johnston et al., 2017, Tab 33.2). A cubic spline interpolation with a "not-a-knot" boundary condition at either end was used to interpolate the position of a GPS satellite between samples.

Then, the performance of the GPS pseudorange observations in combination with the NorSat-TD observations was analysed. At each timestamp of a NorSat-TD observation, the set of visible GPS satellites were identified where the elevation of the satellite was above 10°. From this set of all visible GPS satellites, all unique sub-sequences of three GPS satellites were constructed. These sub-sequences of GPS satellites were then used in combination with the NorSat-TD observation at the given timestamp to estimate the position of the receiver. This estimated position was stored as one of a number of estimated position solutions per timestamp, as there are up to thousands of possible combinations of three GPS satellites for every timestamp. A mean surface position error was then recorded as the mean of the error of all solutions for a given timestamp. Additionally, the standard deviation of this set of position errors was recorded. The same analysis was conducted and results recorded for the HDOP.

Because not all sub-sequences of unique GPS satellites lead to an adequate geometry for a positioning solution, each estimated position was passed through two filters. First, if the geometric DOP (GDOP), that is the square-root of the sum of all elements on the diagonal of $\mathbf{K}^{ENU}$, was higher than 10, the geometry of the three GPS satellites and NorSat-TD was assumed unfit for positioning, and that particular sub-sequence of GPS satellites was neglected from the analysis. An example of such geometry is shown in Figure 4. Secondly, while a given geometry can result in a low evaluation of GDOP, it could still allow ambiguities in the positioning solution, where a local minimum of the optimization problem leads to a positioning solution far away from the true receiver position, appearing as an outlier in the results. To filter out the remaining outlier solutions from the exhaustive set of GPS satellites, a studentized residual approach was used (Thompson, 1935). All estimated positions that deviate beyond three standard deviations from the mean of all recorded position estimates of the current and prior timestamps are discarded. The same is done for the HDOP.

4 | RESULTS

The results following the method in section 3 is presented in three parts, largely reflecting the method. First, the analysis of the characteristics of the VDE-SAT ranging signals is presented in section 4.1. Secondly, the results of the autonomous performance of the various systems of NorSat-TD satellites are presented in section 4.2. Finally, the results of the analysis of a combination of GNSS and VDE-SAT ranging signals are given in section 4.3.

4.1 | Signal Characteristics

The first part of the analysis on the signal characteristics concern the behaviour of the pseudorange residual through a pass. A representative illustration of the measured pseudorange residual through a pass is shown in Figure 5. From this figure it is clear that there is a large negative bias in the residual measurements, and all pseudorange measurements in the pass appear to be approximately 416 km too short. This bias turns out to be common for all pseudorange measurements, across all passes and days. A second observation in Figure 5 is the apparent random noise around an initially decreasing, then increasing trend in the residual measurements. This corresponds partially and inversely with the elevation angle of the satellite as observed by the receiver. This U-shape is visible in four of the eleven passes, where the remaining passes illustrate no or only part of this trend, as seen in Figure 6 with low elevation angles and observations only through part of the pass. All recorded passes show a similar apparent random noise contribution.

When combining all residual measurements, the histogram distribution is as seen in Figure 7, with a mean of −416030.6 m, and a 260.8 m standard deviation. The results are bounded within an approximately 1250 m range. The figure also illustrates the four fitted probability distributions over the histogram, and the KS- and AD-test results are given in Table 5. The AD-test result in a statistic that correspond to a 2.5% confidence in the normality of the distribution, which is below a typical threshold value of 5%. It is also clear from the illustration that the distribution does not have correct tail

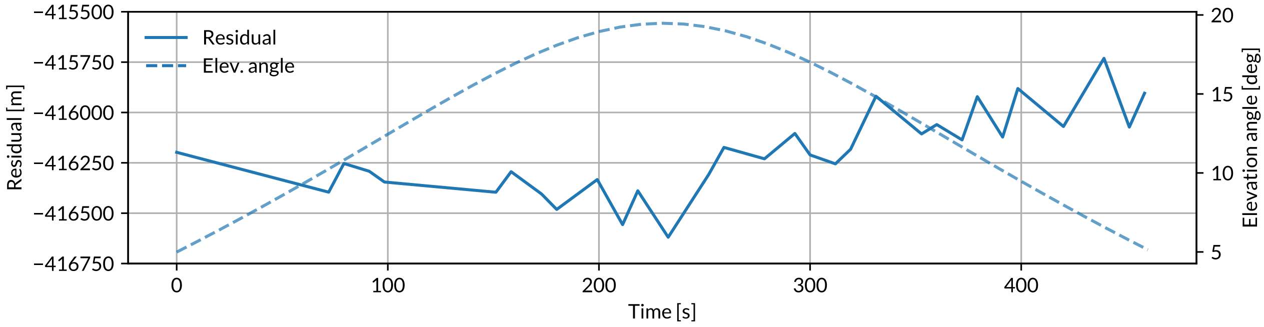

FIGURE 5 The pseudorange residual ϵ_ρ and elevation angle of the satellite over time, of range measurements made during NorSat-TD pass 11/7 - 1, over Trondheim on July 11.

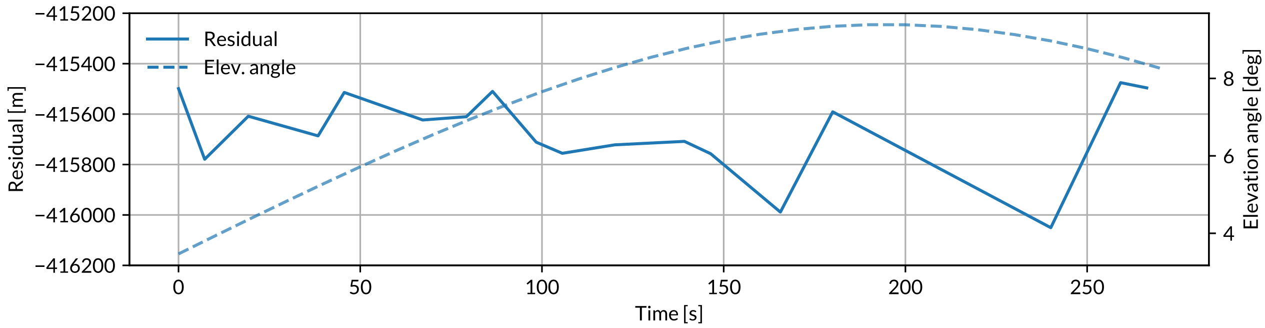

FIGURE 6 The pseudorange residual ϵ_ρ and elevation angle over time, of range measurements made during NorSat-TD pass 25/7 - 3, over Trondheim on July 25.

properties to be considered normal. The KS-test results highlight the Rician distribution as a better fit relative to the other distributions, albeit a small relative difference that is hardly visible in the illustration.

The regression analysis using the four selected parameters gives greater insight in the behaviour of the residual measurements. Figure 8 shows the results of the simple linear regression, which captures the apparent trend of the residual measurements when considering only one parameter. The coefficient results, given in Table 6, show that the correlation between the measured pseudorange (PR) and elevation angle (Elev.) is entirely captured in the models variation with the pseudorange. In the simple linear regression of elevation angle, a clear negative trend is visible, correlating higher elevation angles with smaller residuals. It is apparent from the geometry of the measurements that a higher elevation angle will correlate with a shorter measured pseudorange, which has an equally strong, albeit positive correlation with the residuals in the simple linear regression of the pseudorange. No apparent linear relationship is visible between the SNR and measurement residuals in the simple linear regression, although the results appear to show a heteroscedastic relationship as varying standard deviation in the residuals with SNR. When combining all three parameters in a multiple linear regression, it becomes clear that the correlation between the measured pseudorange and the residuals is a better model for the behaviour of the residuals. A relationship also appears between the SNR and measurement residuals in the multiple linear regression. The intercept of each regression model was around the mean −416 km, and with a very low p-value of < 0.001. The condition number of each model was sufficiently low after normalizing each parameter.

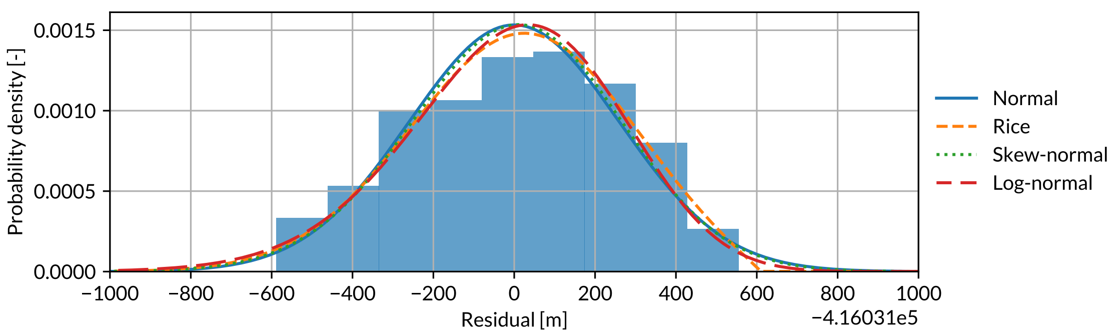

FIGURE 7 A histogram representation of the residual measurements, with the four *normal*, *Rice*, *skew-normal* and *log-normal* probability distributions fitted to the empirical data.

TABLE 5 The results of the KS- and AD-test for the four fitted probability distributions.

Distribution	KS-test (p-value)	AD-test (smallest confidence)
Normal	0.494	0.025
Rice	0.709	-
Skew-normal	0.538	-
Log-normal	0.433	-

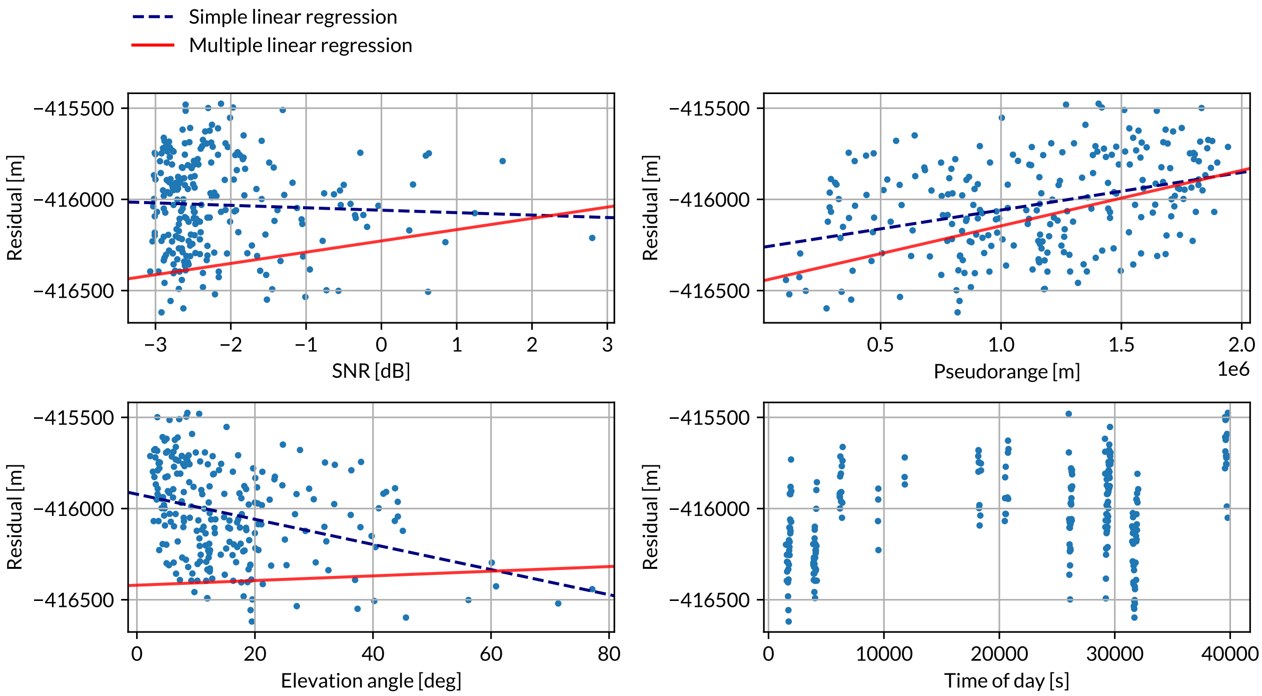

FIGURE 8 All measured pseudorange residuals plotted as a function of the parameters SNR, pseudorange, elevation angle and time of day. The results of the simple and multiple linear regression are presented as trend lines.

The three parameters pseudorange, elevation angle, and time-of-day, are expected to correlate with the residuals due to the effect of the ionosphere. The pseudorange and elevation angle are shown to correlate with each other, but have, both together and separate, considerable correlation with the measured residuals. The residuals are expected to vary as a half-cosine over the time-of-day, but only show a slight increasing trend towards mid-day at $t = 43200$ s. No measurements were obtained in the later half of the day. As for SNR, the increase in the variation in the residuals over the time-of-day shows signs of heteroscedasticity.

After correcting each measurement using one of the three ionospheric correction algorithms, the resulting histogram distributions changed as seen in Figure 9. Two things are immediately clear from this illustration. First, the three ionospheric correction techniques introduce a different-sized bias in the measurements. Secondly, the variation in the residuals only improves for one of the three models. Table 7 show the fundamental statistical description of the four distributions. The NeQuick-G correction technique is the only technique to reduce the standard deviation of the distribution, and it is also the only technique to introduce a significant skew in the distribution while also reducing the kurtosis, making the distribution more normal (albeit skewed).

There are multiple interesting developments to the model fit after applying ionospheric corrections. The KS-test results, reported as p-values, of each distribution applied to the corrected measurements, are shown in Table 8. It is clear from the results that the rudimentary Klobuchar correction technique makes the distribution further distinguishable from the selected probability distributions and adding noise to the distribution. Additionally, the results from the AD-test indicate that the Klobuchar correction entirely removed all confidence in the normality of the distribution, while the NeQuick-G and GIM techniques increase the confidence of the AD-test to $> 15\%$. The NeQuick-G and GIM techniques also show increased p-value for four and three of the distributions, respectively. In particular, the previously highlighted skewed properties of the distribution after applying the NeQuick-G correction is captured remarkably well by the skew- and log-normal distributions. It is also interesting to note how the relatively better fit of the Rician distribution does not appear in the corrected datasets. The behaviour of the histogram distribution changes significantly between ionospheric correction techniques, and only the NeQuick-G correction technique show a reduction in the standard deviation and increase in normality of the distribution.

Applying the NeQuick-G ionospheric correction algorithm reduces the correlations originally revealed in the parametric analysis. The results of

TABLE 6 The computed model coefficients in the simple and multiple linear regression.

Param.	Coefficient	Std. err.	$P > \|t\|$	R^2
Simple linear regression				
Elev.	-515.8	94.9	< 0.001	0.112
SNR	-78.3	107.8	0.468	0.002
PR	378.7	62.2	< 0.001	0.137
Multiple linear regression				
Elev.	95.7	230.7	0.679	0.171
SNR	362.7	117.8	0.002	0.171
PR	559.1	161.0	0.001	0.171

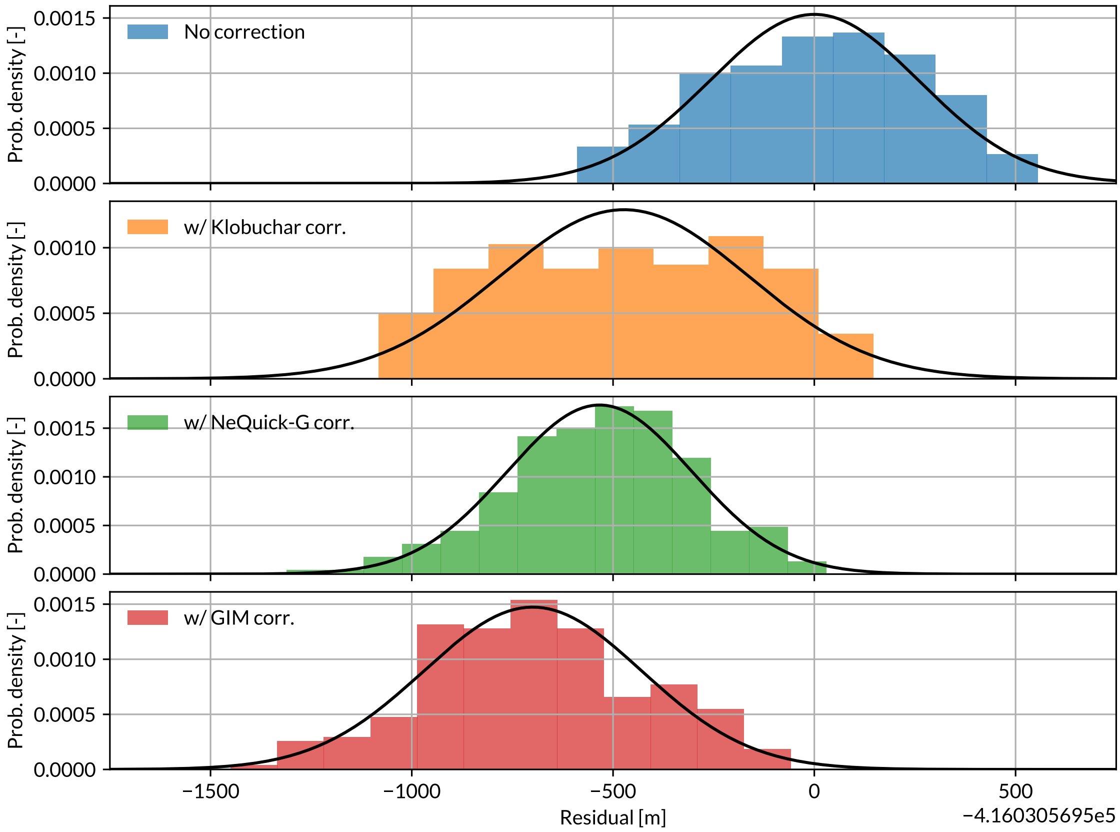

FIGURE 9 Four histogram representations of the residual measurements, with none, or one of the three ionospheric correction algorithms applied to the measurements. Normal distributions are fitted to each histogram to illustrate their difference in mean and variance.

TABLE 7 The fundamental descriptive statistics of the set of residual measurements, with none, or one of the three ionospheric correction algorithms applied to the measurements.

Correction	Mean [m]	St. dev. [m]	Skewness	Kurtosis
No corr.	-416030.6	260.8	-0.0561	-0.782
/w Klobuchar corr.	-416503.2	309.9	-0.0384	-1.054
/w NeQuick-G corr.	-416564.0	230.0	-0.327	0.132
/w GIM corr.	-416730.0	271.4	0.0228	-0.394

TABLE 8 The results of the KS-test (p-value) before and after the three ionospheric correction algorithms are applied, for the four fitted probability distributions.

Distribution	No correction	/w Klobuchar corr.	/w NeQuick-G corr.	/w GIM corr.
Normal	0.494	0.167	0.849	0.904
Rice	0.709	0.158	0.854	0.897
Skew-normal	0.538	0.167	0.992	0.905
Log-normal	0.433	0.132	0.991	0.011

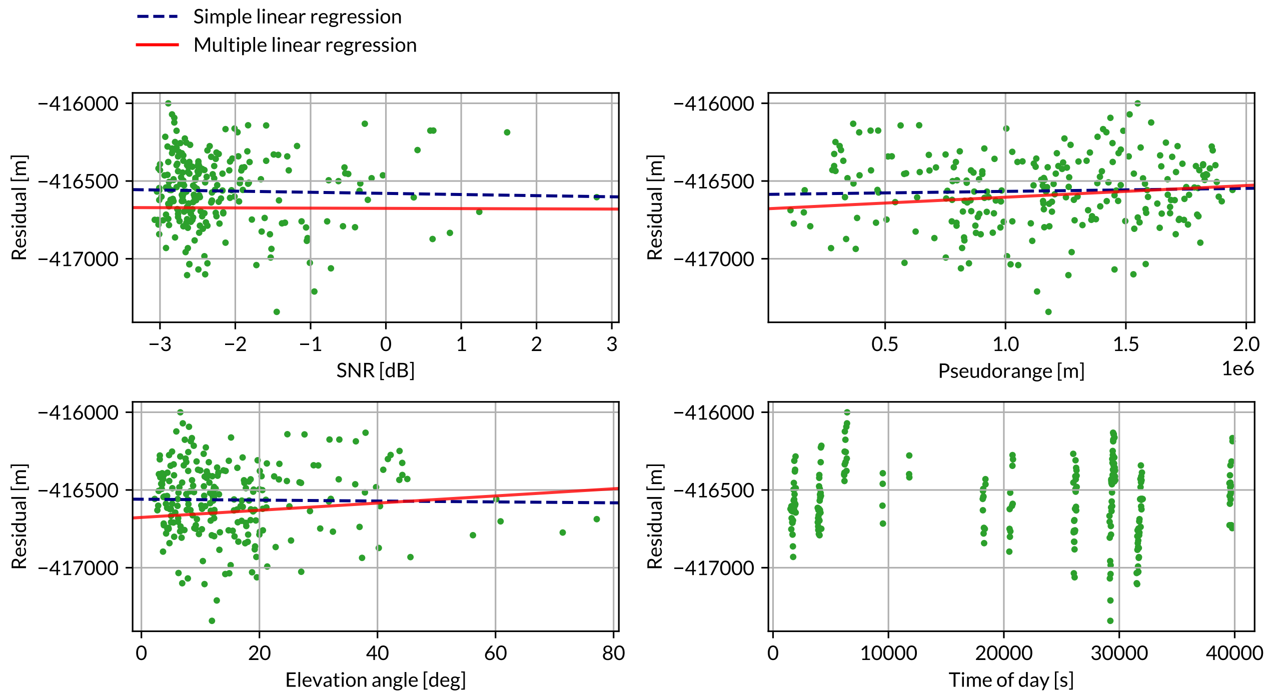

FIGURE 10 All measured pseudorange residuals, corrected for ionospheric time-delay using the NeQuick-G algorithm, plotted as a function of the parameters SNR, pseudorange, elevation angle and time of day. The results of the simple and multiple linear regression are presented as trend lines.

the parametric analysis of the dataset after applying the NeQuick-G correction technique is shown in Figure 10. When comparing the computed trend lines in Figure 10 to that of the uncorrected residuals in Figure 8, it is clear that the NeQuick-G technique largely removes the correlation between the four parameters and the residual measurements. This is also clear from the computed coefficient values presented in Table 9, and the associated p-values of each coefficient, shown in Table 10. The NeQuick-G correction technique significantly reduces the coefficient values of all but one parameter, and show high p-values for all computed parameter coefficients, meaning the influence of the parameter on the residuals can be assumed zero.

The other two correction techniques perform worse than the NeQuick-G technique. Interestingly, the Klobuchar correction technique shows also high p-values in the multiple linear regression, and only for the two parameters of elevation angle and pseudorange, which are associated with the ionospheric time-delay. In the single-parameter simple linear regression, the model is unable to correct for the correlation of these parameters with the residuals, and interestingly seem to over-estimate the influence of the two parameters on the residuals. Both the elevation angle and pseudorange coefficient changes sign, indicating that the Klobuchar correction technique not only corrects, but over-corrects the pseudorange measurements. The Klobuchar correction also introduces a stronger, now positive, correlation between the SNR and the residuals. The GIM technique is entirely unable to correct for the correlations in the parametric analysis, largely increasing coefficient values, and lowering the computed p-values for the elevation angle and pseudorange parameters. The time-of-day variation of the residuals are also affected by the applied correction techniques. As is clear from Figure 10, the NeQuick-G correction reduces the variance in each pass compared to Figure 8, and removes the apparent upwards trend over the time-of-day causing a flattening effect of the time-variation in the residual measurement. This effect appears somewhat after correcting using the Klobuchar technique, but is not present when correcting using the GIM technique.

TABLE 9 A comparison of the computed model coefficients after application of the different ionospheric correction algorithms. Percentages indicate relative absolute size of the new coefficients with respect to the uncorrected coefficients.

Param.	Coefficient	/w Klobuchar corr.	/w NeQuick-G corr.	/w GIM corr.
Simple linear regression				
Elev.	-515.8	339.6 (66%)	-21.6 (4%)	-269.6 (52%)
SNR	-78.3	605.5 (773%)	-42.4 (54%)	-321.7 (411%)
PR	378.7	-243.1 (64%)	35.8 (9%)	297.4 (79%)
Multiple linear regression				
Elev.	95.7	113.3 (118%)	172.5 (180%)	869.2 (908%)
SNR	362.7	561.3 (155%)	-8.8 (2%)	-52.3 (14%)
PR	559.1	14.9 (3%)	138.0 (25%)	809.2 (145%)

TABLE 10 A comparison of the computed coefficient p-values after application of the different ionospheric correction algorithms.

Param.	$P > \|t\|$	/w Klobuchar corr.	/w NeQuick-G corr.	/w GIM corr.
Simple linear regression				
Elev.	< 0.001	0.004	0.808	0.010
SNR	0.468	< 0.001	0.656	0.004
PR	< 0.001	0.002	0.544	< 0.001
Multiple linear regression				
Elev.	0.679	0.692	0.440	0.001
SNR	0.002	< 0.001	0.939	0.678
PR	0.001	0.941	0.376	< 0.001

4.2 | Autonomous VDE-SAT Positioning Performance

The evaluation of the autonomous positioning performance of VDE-SAT starts with the rolling performance assessement using only the NorSat-TD VDE-SAT range observations. The result of this method for a varying number of consecutive observations N is shown in Figure 11, plotted on a log-scale. The performance is plotted both with and without the use of a ground constraint, for each of the recorded passes. Both the results with and without ground constraint show a downwards trend with increasing number of observations, and the surface position errors with ground constraint are consistently $10 - 100$ times smaller than for the errors obtained with no ground constraint. The lowest computed surface position error with no ground constraint is about 6 km. For $N > 17$, positioning with a ground constraint results in surface position error around or below 1000 m for all passes with at least as many observations, bar one pass with an error at about 9 km. For the two passes with more than 30 observations, there is little improvement in the surface position error for $N > 30$, both with and without the ground constraint.

The two constellations are simulated and observations gathered at specific timestamps with an added noise and bias contribution equal to that of the uncorrected signal given in Table 7, as a worst case performance. The resulting observations at the receiving antenna revealed some geometric

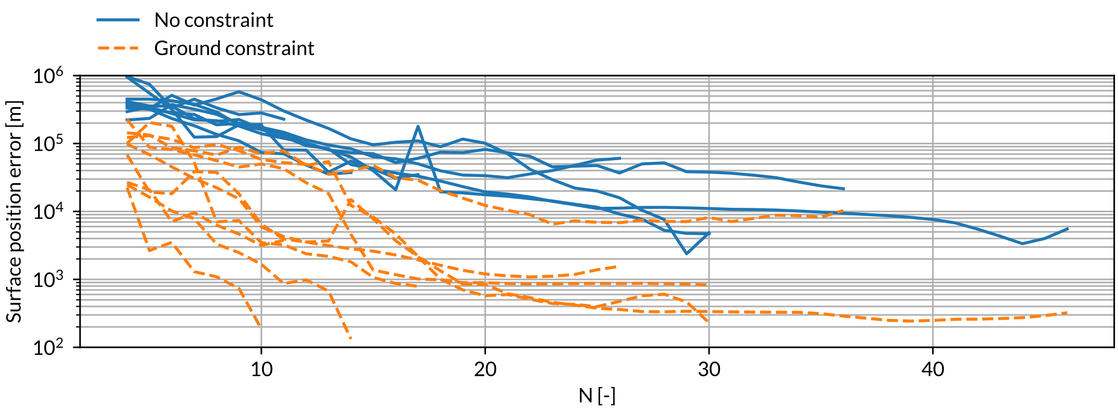

FIGURE 11 All passes equated with a *mean rolling performance* metric, for a varying number of observations N.

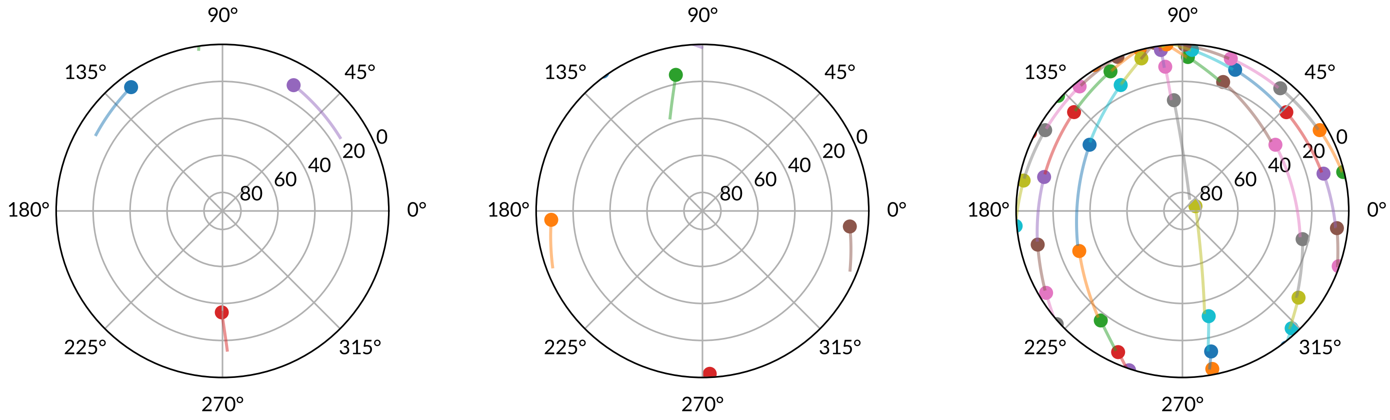

(a) An example of three satellites visible above a receiver in the Iridium constellation.

(b) An example of four satellites visible above a receiver in the Iridium constellation.

(c) The large number of visible satellite above a receiver in the OneWeb constellation.

FIGURE 12 Three sky plots for various scenarios in the Iridium and OneWeb constellations. Azimuthal directions around, and elevation angles in degrees are shown radially towards the center.

TABLE 11 The mean surface position error of the two simulated constellations, with and without a ground constraint.

Constellation	Mean [m]	Mean, /w ground constraint [m]
Iridium	903.2	337.5
OneWeb	77.5	77.3

issues for the Iridium constellation. As shown in Figure 12a, at certain times only three satellites of the Iridium constellation are visible above the receiver, making positioning impossible at this epoch. However, about equally common is a geometry as shown in Figure 12b, where four satellites are visible above the receiver. If a ground constraint is employed these geometries will typically improve, although there is still the occasional geometry where a satellite is observed directly above the receiver. This means the direction of the observation in question and ground constraint will coincide, which in turn may result in rank deficiency in the design matrix, making positioning impractical. Also shown in Figure 12c is the large number of visible satellites above the receiver in the simulated OneWeb constellation. There are typically over 20 satellites above the horizon at any point in time. No rank deficiency is experienced when performing positioning with this constellation.

Figure 13a shows the surface position error performance of the Iridium constellation simulated over 24 hours. From this figure we can see two interesting details. First, what stands out is the large difference in coverage with and without the ground constraint over these 24 hours. Less than half of the time there is a valid positioning solution, visible as gaps in the resulting surface position error. This improves significantly with a ground constraint, although there are still significant periods with no coverage, likely because of a geometry of three satellites as shown in Figure 12a, where one of three visible satellites pass directly above the receiver, causing the direction of the observation to approximately coincide with the ground constraint. Second, the surface position error appears as a noise contribution around an approximate mean, measured equal to 903.2 m without, and 338.3 m when including a ground constraint, given in Table 11. This is similar to the results given in (Owens et al., 2021, Fig. 9) for a comparable emulation of the Iridium constellation in combination with a ground constraint or ground-based observations, as is the case for the results of Owens et al. (2021). Figure 14 shows the surface position error performance at the receiver under the OneWeb constellation over the same 24 hours. Immediately it is clear that the large coverage shown in Figure 12c contributes to a much lower error level, which is below 100 m for over 70% of the position evaluations. The ground constraint does not significantly influence the results. The resulting mean surface position errors under the two constellations are reported in Table 11.

Figure 13b shows the HDOP of the Iridium constellation with a ground constraint over the same timespan as in Figure 13a. With over 92% of the results in the interval [1.0, 2.0], the computed HDOP is similar to that seen in (Owens et al., 2021, Fig. 9) for their similarly emulated Iridium constellation. It is then interesting to note that the computed surface position error in Figure 13a shows a significantly lower upper error level than that seen in the work of Owens et al. (2021), at the same geometric performance.

4.3 | VDE-SAT performance as contemporary backup service

Figure 15 shows the positioning performance for an example pass when using NorSat-TD as a backup service. The pass is the first pass of July 11th, for which the residual has been presented in Figure 5. It is apparent that the surface position error follows closely the measurement residual through the pass. In contrast, it does not seem to correlate with changes in the HDOP, as seen in Figure 15. This trend where the surface position error closely follow the absolute measurement residual is true for all passes, meaning all passes measure a mean error near or below the standard deviation of a single range measurement, as seen in Table 12. This can be understood as the least-squares solution of the four estimated state parameters with four observations is able to return a solution where all least-squares residuals are equal to zero. This includes the NorSat-TD pseudorange, so the large

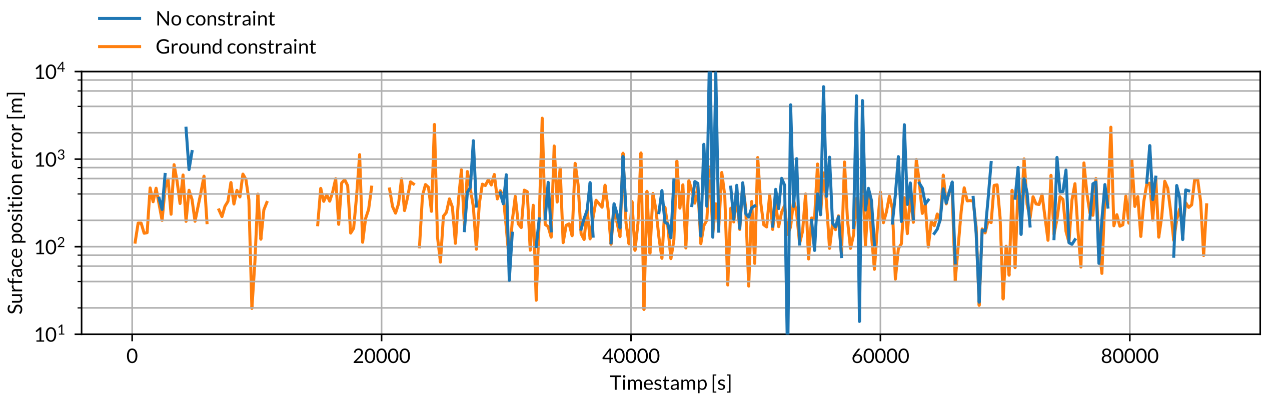

(a) Surface position error in the estimated state over time, using a simulated Iridium constellation.

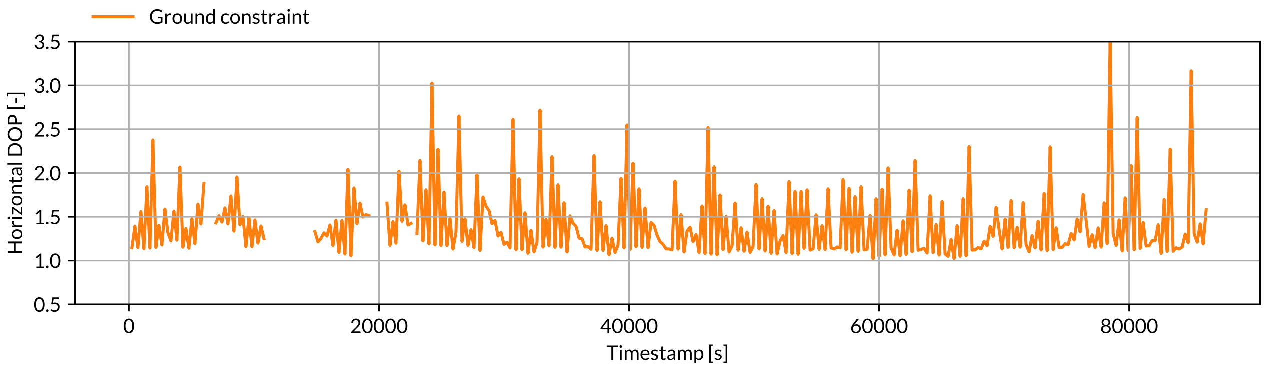

(b) Horizontal DOP at the user over time, in the simulated Iridium constellation, with a ground constraint.

FIGURE 13 The central positioning performance metrics for the simulated Iridium constellation.

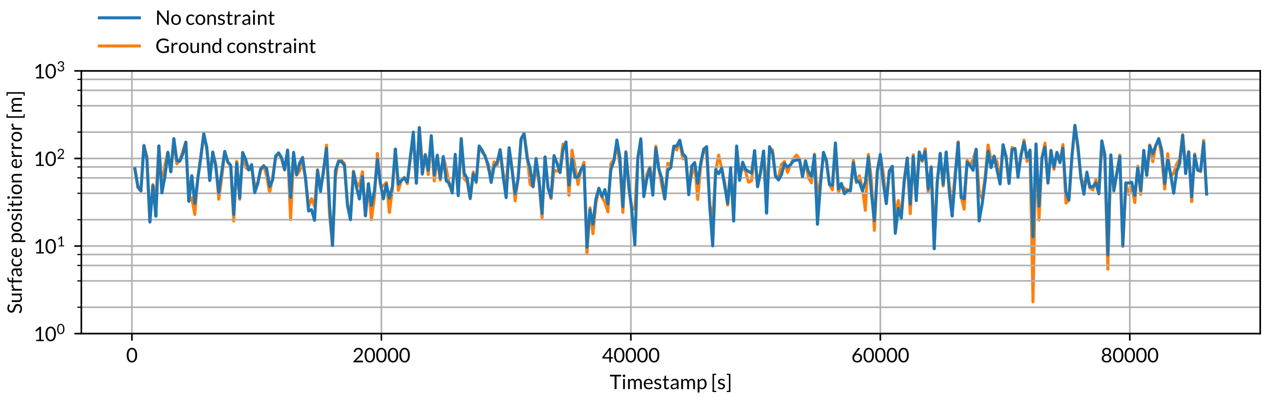

FIGURE 14 Horizontal position error in the estimated state over time, using a simulated OneWeb constellation.

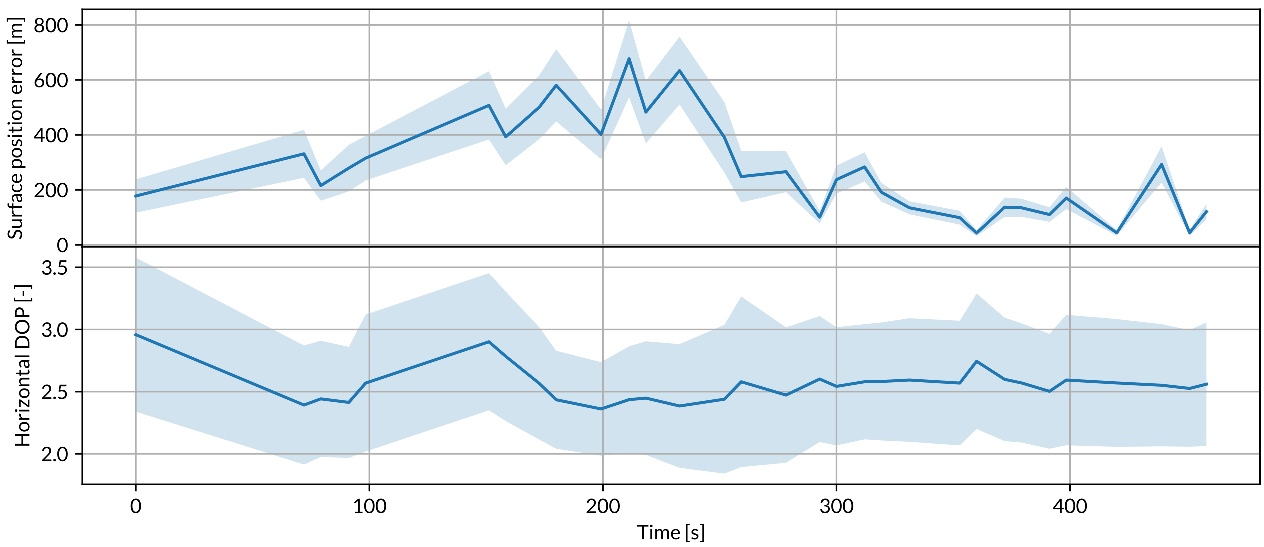

FIGURE 15 The mean horizontal position error in the estimated state and HDOP over time, equated at each timestamp for a variation in constellations combined of three GPS-, and one VDES-satellite. One standard deviation is shown as a transparent area above and below the mean at each timestamp.

VDES range error compared to the GPS range errors dominates the surface position error. The performance metrics are listed per pass in Table 12, and the total mean surface position error is equated to 218.2 m, with a 212.4 m standard deviation from the varying geometries.

The filter performance given in Table 12 show that even if three GPS satellites are supplemented by a NorSat-TD observation, it is not necessarily sufficient for a valid positioning solution. The combination of those particular GPS satellites and a low-orbiting NorSat-TD can result in a geometry where the GDOP is (often much) larger than 10, which is impractical for positioning at any accuracy. Of all combinations of three visible GPS satellites and one NorSat-TD observation at each observation timestamp, only about 60.7% of them result in geometry which can be considered valid. This is also true for each pass individually, as all passes eliminate nearly around half of the exhaustive list of geometries, seen in Table 12 as similar ratios eliminated by the geometric filter. Further, of the geometries that make it through this filter, only 95.9% make it through the filter of studentized residuals which remove all results further than three standard deviations away from the accumulated mean surface position error. This filter removes a small number of results in each pass, where a significant number are associated with the discussed possible ambiguities of the optimization problem, meaning the resulting surface position error is typically on the scale of tens of kilometres and is detectable as an outlier. That leaves approximately 58.3% of all possible combinations of three GPS measurements with the empirical NorSat-TD observations as valid for positioning, with a mean surface position error well below the listed requirement for navigation on the ocean, seen in Table 4.

5 | DISCUSSION

This section will present a discussion of the results in section 4. The initial objective of the project has been to achieve better understanding of the characteristics, limitations and possibilities of VDE-SAT pseudoranges as a source of PNT in the Arctic. This discussion will first consider the results on the signal characteristics, and draw conclusions on the contribution of propagation errors on the ranging performance. Further this discussion will use the results and assumptions of the system performance analysis to evaluate the use of VDE-SAT as a GNSS backup or contingency service.

5.1 | Signal characteristics

When first analysing the behaviour of the computed residuals through a pass, this study found that a number of passes exhibited a U-shape variation as the NorSat-TD satellite passed overhead. This U-shaped contribution has been shown to be larger than the inherent noisy contribution to the range measurements in four of the eleven passes considered. Considering the geometry of a satellite pass, this reduction in the residual mid-pass correlates with a shorter time-of-flight, making it reasonable to assume the U-shape variation is due to propagation effects. These results show that an important aspect of the behaviour of VDE-SAT pseudoranges are effects due to the signal propagation. Further, the study shows that the measured pseudorange residuals have a large, but stable, bias over the month of July. This is believed to be due to a static transmit bias, which is known to be entirely uncorrected in the current implemented firmware on-board NorSat-TD, and not be due to propagation effects. This bias is easily correctable through a navigational message entry.

The histogram distribution of the uncorrected residuals does not conform to an expected probability distribution. The leading hypothesis has been that the pseudorange error will follow a largely normal distribution, as is the case for traditional GNSS (Kaplan and Hegarty, 2006). Šafář et al. (2021) has also highlighted multipath error as a possible critical source of noise in VDE-SAT ranging signals, which has been shown to follow a Rician distribution in maritime environments (Sandrin and Fang, 1986). However, the finding of this study is contrary to both of these hypotheses, as the

TABLE 12 The surface position error performance for each pass acting as a GNSS backup service, and the summarizing total performance metrics of all passes combined. The geometric (geom.) filter describes the number of geometries with HDOP below 10.0, and the studentized (stud.) filter describes the number of the remaining geometries where the mean positioning error was not an outlier. Values in bracket indicate the total fractional percentage of geometries that pass the filter.

Pass	Pos. error, mean [m]	Pos. error, st. dev. [m]	Geom. filter	Stud. filter
11/7 - 1	225.2	209.6	1130 / 2604	1109 / 1130
11/7 - 2	208.1	189.6	1763 / 2640	1749 / 1763
11/7 - 3	216.8	184.0	4715 / 7755	4559 / 4715
18/7 - 1	186.1	131.0	1162 / 1792	1121 / 1162
18/7 - 2	88.3	72.0	294 / 480	279 / 294
18/7 - 3	89.8	95.6	706 / 1028	656 / 706
18/7 - 4	188.4	165.9	947 / 1764	930 / 947
18/7 - 5	243.6	266.8	4799 / 7920	4525 / 4799
25/7 - 1	111.3	94.0	1588 / 2475	1470 / 1588
25/7 - 2	263.1	183.1	283 / 495	279 / 283
25/7 - 3	337.9	240.3	2003 / 2970	1919 / 2003
Total	**218.2**	**212.4**	**19390 / 31923** (60.7%)	**18596 / 19390** (95.9%)

presented distribution of residuals do not satisfy common tests for normality, nor does it show considerable fit to the alternative distributions, including the Rician distribution. This again could point to a correctable error in the residuals, which introduces a systematic (not noisy) error contribution on an otherwise normal distribution, causing the histogram distribution to deviate from its expected shape.

Two key results now show a connection to a significant propagation delay, and it is further shown in the parametric analysis that this may be the time-delay due to the ionosphere. Of the four parameters included in the analysis, three are expected to correlate with a theoretical ionospheric time-delay, namely the pseudorange, elevation angle, and time-of-day. When the pseudorange and elevation angle are included in a simple and multiple linear regression model of the variation in the residual, this study found significant correlations between these parameters and the measured residuals. Similarly, the residual variation appear to match the expected half-cosine variation with time-of-day, although these results are less conclusive, as measurements are only made in approximately the first half of the day. This type of correlation is not found to be significant in another parameter that is not expected to largely correlate with the ionospheric time-delay, namely SNR. It seems possible that these results point to the propagation delay being time-delay due to the propagation through the ionosphere.

Further results pointing to the ionospheric time-delay is the successful application of ionospheric correction techniques. Of the three models applied, the two Klobuchar and GIM techniques are based on a thin shell model, assuming the total effect of the ionosphere appears as a thin shell at a set, low, altitude. This is because traditional GNSS satellites lie above the ionosphere, making this assumption reasonably valid. However, as the LEO satellites, and in this case NorSat-TD, lie *inside* the ionosphere, the assumption that all of the ionosphere acts on the propagated signal is not believed to be valid. This is also supported by literature, where the issue of ionospheric bottomside modelling using LEO satellites is done by scaling down the vertical TEC reported in available thin shell models (Li et al., 2022). Because this is not done in the Klobuchar and GIM techniques, an overestimation of the effect due to the ionosphere appears in the results. First, the simple linear regression after application of the Klobuchar technique shows that the computed model coefficients capture the entirely opposite trend of the uncorrected residuals. This can be connected to the overestimation of the thin shell model and in turn the correlation of the parameters with the now corrected residuals. The GIM technique is largely unable to reduce any effect of the parameters on the residuals, but the change in the mean of the distribution is by far the largest of the three applied corrections, which also point to an overestimation. However, the one model that does not implement a thin shell model does not appear to overestimate the effect of the ionosphere.

The NeQuick-G correction technique uses a variable height ionospheric electron density model, which appears to eliminate the issues associated with the thin shell model, and the result is a more accurate range measurement. This technique reduces the correlation between the selected parameters and the residuals, as well as reducing the overall standard deviation of the histogram distribution. Additionally, the NeQuick-G-corrected data distribution is shown to have a high degree of normality, and a significant fit to the skew- and log-normal distribution. These results show that the NeQuick-G ionospheric correction technique is directly applicable to VDE-SAT pseudoranges as a correction for propagation delay. The result is a nearly normal distribution of residuals, which can be associated with the expected Gaussian noise contribution of a pseudorange signal. The resulting standard deviation of about 230 m is still significantly higher than the estimated performance bound of 82.2 m, but considering that this corresponds to a lower bound estimate, which according to Šafář et al. (2021) neglects realistic additional error, the normality of the corrected distribution is a good indication this is close to the inherent noisy error of VDE-SAT pseudorange measurements. These results shows that the VDE-SAT pseudoranges are significantly affected by ionospheric propagation delay. This is as expected as the VDE-SAT pseudoranges are sent at about a tenth of the frequency of GNSS, making them more vulnerable to dispersion. Ionospheric correction techniques designed specifically for VDES frequencies could aid in the mitigation of these propagation effects.

5.2 | System performance analysis

The performance of the current capabilities of NorSat-TD acting as an autonomous PNT-source has several significant assumptions. An important limitation of the current system is the dependency on GNSS for accurate timing and positioning of the satellite. A fundamental assumption is that both the transmitting satellite and the receiver are time-synchronized to GNSS. This is a requirement for the current VDES ground infrastructure, as well as a requirement for the accurate positioning of NorSat-TD. For relatively short GNSS-outages, the holdover capabilities of the onboard clock, as well as accurate propagation of the satellite may be sufficient for a contingency system, but this is beyond the scope of this work. The implications of these assumptions are not explored in this work, but the cases presented are still realistic for a case of partial coverage in a contemporary system, or a further developed complete constellation of satellites with VDE-SAT capabilities. However, as a note of caution, the conclusions of this work are based on assumptions of sufficient GNSS coverage for the positioning of the transmitting satellite, and for time dissemination at the receiver (Lewandowski and Thomas, 1991).

The equated performance of the contemporary single satellite system does not consistently fit the requirements for a navigation backup system. This is expected, as any single-satellite system, even with higher ranging accuracy, will not lead to good positioning performance. Issues related to single-satellite positioning are well-known in literature (Levanon, 1999; Chen et al., 2016). Using a method similar to that of Chen et al. (2016), the evaluated mean surface position error is not below the requirements for a general navigation backup system, seen in Table 4. With the application of a ground constraint, it is possible, however not consistently, to position within the required 1000 m for navigation at ocean. However, six of the eleven satellite passes do result in a positioning solution within this requirement, which is an interesting find for further developments of the system, as this is a key metric that will serve as an important benchmark for the next iteration of navigation systems using VDE-SAT.

When simulating the Iridium constellation with the equated VDE-SAT ranging accuracy, a mean surface position error of 338.3 m would fall well under the requirement for backup navigation at ocean. As is also found in the feasibility study of Owens et al. (2021), a medium-sized constellation is a possible system design for a continuously available VDE-SAT navigation backup system. In contract to the conclusions of Owens et al. (2021), these findings show that with even a rudimentary ground constraint, the positioning performance fall under the requirements for navigation at ocean, also beyond mid-latitudes. Further, the simulated OneWeb mega constellation is shown to result in significantly improved positioning performance even with the current signal performance. With a mean surface position error below 100 m, and with robust integrity, a mega constellation of contemporary VDE-SAT capable satellites would fulfil the requirements for navigation at ocean as well as along the coast, as defined in Table 4. This is a significant performance increase, in contradiction to the conclusions of Owens et al. (2021) on the possible improvements with a mega constellation. However, with many hundreds of satellites required for such a constellation, and with no concern for the complex channel coordination of VDES, this is at best a solution for the far-future. A key assumption of the system performance analysis is the stable 550 km altitude of the simulated constellations, which differs from the realistic orbit of NorSat-TD. After launch, the satellite was found to orbit closer to a 500 km altitude, with significant eccentricity. However, this is not expected to significantly influence the results. The results of this analysis are conservative measures of the system performance as they are based on the current, uncorrected ranging accuracy of VDE-SAT, which may significantly improve in the future.

The positioning performance obtained with various constellations show that new developments of VDE-SAT systems can contribute to a valid general navigation backup systems under the given assumptions. In previous studies, the discussed single-satellite system was considered feasible for adequate positioning performance in combination with terrestrial VDE-TER systems (Owens et al., 2021). The findings of this work supports this conclusion, and confirms that such a system is feasible with the current performance of VDE-SAT ranging, meaning developments to extend this system with additional satellites for continuous coverage could be sufficient for a navigation backup system. Secondly, the two simulated constellations confirms that further developments with the current signal performance can become a viable general navigation backup system, with positioning performance below the requirements for both oceanic and coastal navigation, for a medium and mega constellation, respectively.

The current performance of VDE-SAT ranging is shown to deliver in about 60% of the cases a positioning accuracy within 1000 m, in the event of partial GNSS coverage. The results of section 4.3 show that in case only three GNSS satellites are available, the use of VDE-SAT range observations can allow for valid positioning at an approximate 60% of the considered geometries, which means such as system can act as a contingency system, as an alternative to no navigation system at all. The geometric filter leading to the equated 60% valid positioning solutions is also a conservative measure. The considered geometries are exhaustive of all visible satellites over Trondheim, some of which would not be considered in the Arctic where the few visible satellites are expected to form a better geometry for the user than some of the ones considered in this analysis. The implication of this can be crucial for critical navigation in the Arctic, enabling user positioning under the common scenario of only partial GNSS coverage. In this regard, the operation of more VDE-SAT satellites over the Arctic is key in the development of such a contingency system. Additionally, the positioning performance is found to correlate directly with the accuracy of the range measurements, meaning developments on the ranging accuracy of VDE-SAT will also directly contribute to the performance of this contemporary contingency system.

6 | CONCLUSION & FURTHER WORK

This study had the aim to achieve a better understanding of the contemporary characteristics, limitations and future possibilities of VDE-SAT pseudo-range measurements acting as a PNT-source. This was done by means of a statistical analysis of in total 236 VDE-SAT range measurements obtained from the recently launched NorSat-TD satellite, and a performance analysis of various systems of simulated VDE-SAT capable satellites. The results indicate that the previously neglected effect of propagation on a VDE-SAT range measurement is significant, and likely due to the time-delay due to the ionosphere. It is also shown that this effect is to some extent correctable using the NeQuick-G ionospheric correction model, due to its consideration of variable transmitter altitude, in contrast to other ionospheric correction models. The resulting estimated range error is 260.8 m and 230.0 m before and after the application of the NeQuick-G correction model. The pseudorange measurements also have a large and constant mean error of about 416 km. VDE-SAT as a PNT-source can contribute to a possible future general navigation backup system. It is also shown that the performance of such a backup system is largely dependent on the available satellite infrastructure, but medium-size constellations with geometrical constraints for the user can result in consistent coverage and a positioning performance below 1000 m. Finally, an important conclusion of this study is that a contemporary navigation contingency system is feasible with the current NorSat-TD satellite in the event of partial GNSS coverage in the Arctic, allowing for user positioning within 1000 m. This provides a goal for the further development of the system, and consistent and robust positioning with a 1000 m accuracy is recommended as a target metric for future iterations of VDE-SAT positioning systems. This study has successfully presented the ranging performance of VDE-SAT ranging signals, and evaluated the characteristics of its error distribution. Further, the study successfully concludes on the future possibilities of VDE-SAT as a PNT-source, and has demonstrated the contemporary opportunities of the currently available system.

The fundamental assumptions of a GNSS-positioned transmitter and time-synchronized receiver should be answered in later iterations of the system design. Questions regarding the clock and position drift, in the case the VDES-infrastructure is not GNSS-disciplined, remain unanswered, as they were not the topic of this analysis. However, these assumptions are not believed to largely affect the conclusions of the performance analysis, as the possible error in a truly autonomous system, for example using ground-based orbit determination and timing, is likely less than the inherent noise of the VDE-SAT range measurements. Still, the topic of this and following research is limited to only a semi-autonomous system until global VDES infrastructure is considerably developed.

The conclusion of the analysis of corrections is unable to conclusively establish the time-delay due to the ionosphere as the definitive source of error in the measurements due to the remaining variance in the distribution. The analysis was limited to ionospheric correction techniques, chosen in favour of other propagation effects based on the conclusions of related literature (Owens et al., 2021). While the results show a clear indication that the ionospheric delay is the only systematic signal error larger than the inherent noise of the signal, a different method investigating a wider set of error contributions could lead to a more definite conclusion on the error contributions of a VDE-SAT pseudorange. These contributions could be the effect of the troposphere, which contributes a similar, albeit smaller, time-delay to the ranging signals. It is also hypothesized in Šafář et al. (2021) that multipath error can have a significant effect on VDE-SAT ranging signals. A recommended further topic is the investigation of the contribution of different error sources in the system using more sophisticated measurement techniques such as single- and double-differencing, and the development of VDES-specific correction techniques for known systematic errors such as the time-delay due to the ionosphere.

Considerably more analysis is be needed to fully investigate a possible contemporary contingency service using VDE-SAT. The current analysis is limited to the combination of three GPS observations with exactly one observation from NorSat-TD. This significantly limits the scope of the results, which should not be considered more than an early indication of positive feasibility for the concept of VDE-SAT acting as a GNSS contingency service. Further work on this topic should broaden the scope by considering variations in number and type of GNSS satellites, as well as VDE-SAT and VDE-TER PNT-sources.

Further experimental investigations are needed for validation of these results. Obtaining a larger dataset of VDE-SAT pseudorange observations can provide larger confidence in the results of the statistical analysis, and also provide answers to the variation of the standard deviation of the range measurements with parameters such as the SNR. This analysis was limited to a single static receiver in Trondheim, Norway, and more empirical data from different environments and different ground station setups of antennas will greatly supplement this research. Additionally, experiments using a dynamic receiver are recommended, as conclusions may change between a static receiver and a dynamic receiver, which are more applicable for ships in a maritime environment.

acknowledgements

This paper is written as part of a thesis paper submission to obtain the degree of Master of Science at the Delft University of Technology, in collaboration with Space Norway and Kongsberg Seatex. Thanks to thesis supervisor Jose van den IJssel and Sven-Ingve Rasmussen for their support.

data & software acknowledgements

GPS precise orbit and GIM products were available through the International GNSS Service (IGS)[6]. These products were accessed through the Crustal Dynamics Data Information System (CDDIS) repository[7]. The distributed ionospheric correction coefficients, as well as GPS observations for validation routines were accessed through the ESA GNSS Science Support Center (GSSC), and in particular their platform "GSSC Now"[8]. The official source code of the NeQuick-G algorithm was made available to this work by the European GNSS Service Centre[9].

references

Anderson, T. W. and Darling, D. A. (1952) Asymptotic Theory of Certain "Goodness of Fit" Criteria Based on Stochastic Processes. *The Annals of Mathematical Statistics*, **23**, 193–212.

Breivik, K., Forssell, B., Kee, C., Enge, P. and Walter, T. (1997) Estimation of Multipath Error in GPS Pseudorange Measurements. *Navigation*, **44**, 43–52.

[6]URL `https://igs.org/products/`, Accessed 03/10/2023.
[7]URL `https://cddis.nasa.gov/archive/gnss/products/`, Accessed 03/10/2023.
[8]URL `https://gssc.esa.int/`, Accessed 03/10/2023.
[9]URL `https://www.gsc-europa.eu/support-to-developers/ionospheric-correction-algorithms/nequick-g-source-code`, Accessed 03/10/2023.

Bullock, R. (2007) Great circle distances and bearings between two locations. *MDT*.

Chen, X., Wang, M. and Zhang, L. (2016) Analysis on the Performance Bound of Doppler Positioning Using One LEO Satellite. In *2016 IEEE 83rd Vehicular Technology Conference (VTC Spring)*, 1–5. Nanjing: IEEE.

DeCleene, B. (2000) Defining pseudorange integrity-overbounding. In *Proceedings of the 13th International Technical Meeting of the Satellite Division of The Institute of Navigation (ION GPS 2000)*, 1916–1924.

European Commission (2016) Ionospheric correction algorithm for GALILEO single frequency users.

Grejner-Brzezinska, D. A., Wielgosz, P., Kashani, I., Smith, D. A., Spencer, P. S. J., Robertson, D. S. and Mader, G. L. (2004) An analysis of the effects of different network-based ionosphere estimation models on rover positioning accuracy. *Journal of Global Positioning Systems*, **3**, 115–131.

Griffiths, J. (2019) Combined orbits and clocks from IGS second reprocessing. *Journal of Geodesy*, **93**, 177–195.

Hu, W. and Farrell, J. A. (2019) Technical Note: Derivation of Earth-Rotation Correction (Sagnac) and Analysis of the Effect of Receiver Clock Bias. *Technical note*, UC Riverside, Riverside, CA.

IALA (2012) R0129 GNSS VULNERABILITY AND MITIGATION MEASURES, Edition 3.1.

— (2019) G1139 THE TECHNICAL SPECIFICATION OF VDES, Edition 3.

ITU-R (2022) Recommendation ITU-R M.2092-1: Technical characteristics for a VHF data exchange system in the VHF maritime mobile band.

James, G., Witten, D., Hastie, T. and Tibshirani, R. (eds.) (2013) *An Introduction to Statistical Learning: With Applications in R*. No. 103 in Springer Texts in Statistics. New York: Springer.

Johnson, G. and Swaszek, P. (2014) The Feasibility of R-Mode to Meet Resilient PNT Requirements for e-Navigation. In *27th International Technical Meeting of the Satellite Division of the Institute of Navigation, ION GNSS 2014*. Tampa, FL.

Johnston, G., Riddell, A. and Hausler, G. (2017) The International GNSS Service. In *Springer Handbook of Global Navigation Satellite Systems* (eds. P. J. Teunissen and O. Montenbruck), 967–982. Cham: Springer International Publishing.

Kaplan, E. D. and Hegarty, C. (eds.) (2006) *Understanding GPS: Principles and Applications*. Artech House Mobile Communications Series. Boston: Artech House, 2nd ed edn.

Klobuchar, J. (1987) Ionospheric Time-Delay Algorithm for Single-Frequency GPS Users. *IEEE Transactions on Aerospace and Electronic Systems*, **AES-23**, 325–331.

Levanon, N. (1999) Instant Active Positioning with One LEO Satellite. *Navigation*, **46**, 87–95.

Lewandowski, W. and Thomas, C. (1991) GPS time transfer. *Proceedings of the IEEE*, **79**, 991–1000.

Li, T., Wang, L., Fu, W., Han, Y., Zhou, H. and Chen, R. (2022) Bottomside ionospheric snapshot modeling using the LEO navigation augmentation signal from the Luojia-1A satellite. *GPS Solutions*, **26**, 6.

Milliken, R. J. and Zoller, C. J. (1978) Principle of Operation of NAVSTAR and System Characteristics. *Navigation*, **25**, 95–106.

Montenbruck, O., Steigenberger, P. and Hauschild, A. (2018) Multi-GNSS signal-in-space range error assessment – Methodology and results. *Advances in Space Research*, **61**, 3020–3038.

Moré, J. J. (1978) The Levenberg-Marquardt algorithm: Implementation and theory. In *Numerical Analysis* (ed. G. A. Watson), vol. 630, 105–116. Berlin, Heidelberg: Springer Berlin Heidelberg.

O'Hagan, A. and Leonard, T. (1976) Bayes estimation subject to uncertainty about parameter constraints. *Biometrika*, **63**, 201–203.

Owens, A. J., Richardson, T. and Critchley-Marrows, J. (2021) The Feasibility of a VDE-SAT Ranging Service as an Augmentation to GNSS for Maritime Applications. In *34th International Technical Meeting of the Satellite Division of The Institute of Navigation (ION GNSS+ 2021)*, 591–616. St. Louis, Missouri.

Šafář, J., Grant, A. and Bransby, M. (2021) Performance bounds for VDE-SAT R-Mode. *International Journal of Satellite Communications and Networking*.

Šafář, J., Grant, A., Williams, P. and Ward, N. (2020) Performance Bounds for VDES R-mode. *Journal of Navigation*, **73**, 92–114.

Šafář, J., Shaw, G., Grant, A., Haugli, H. C., Løge, L., Christiansen, S. E. and Alagha, N. (2018) GNSS Augmentation using the VHF Data Exchange System (VDES). In *31st International Technical Meeting of The Satellite Division of the Institute of Navigation (ION GNSS+ 2018)*, 1788–1805. Miami, Florida.

Sandrin, W. A. and Fang, D. J. (1986) Multipath fading characterization of L-band maritime mobile satellite links. *COMSAT Technical Review*, **16**, 319–338.

Sheng-Ju, S. (2015) Implementation of Cyclic Redundancy Check in Data Communication. In *2015 International Conference on Computational Intelligence and Communication Networks (CICN)*, 529–531. Jabalpur, India: IEEE.

Shiryayev, A. N. (1992) On The Empirical Determination of A Distribution Law. In *Selected Works of A. N. Kolmogorov* (ed. A. N. Shiryayev), 139–146. Dordrecht: Springer Netherlands.

Stephens, M. A. (1974) EDF Statistics for Goodness of Fit and Some Comparisons. *Journal of the American Statistical Association*, **69**, 730–737.

Thompson, W. R. (1935) On a Criterion for the Rejection of Observations and the Distribution of the Ratio of Deviation to Sample Standard Deviation. *The Annals of Mathematical Statistics*, **6**, 214–219.

Tietjen, G. L., Moore, R. H. and Beckman, R. J. (1973) Testing for a Single Outlier in Simple Linear Regression. *Technometrics*, **15**, 717–721.

Wirsing, M., Dammann, A. and Raulefs, R. (2019) Investigating R-Mode Signals for the VDE System. In *OCEANS 2019 MTS/IEEE SEATTLE*, 1–5. Seattle, WA, USA: IEEE.

— (2023) VDES R-Mode performance analysis and experimental results. *International Journal of Satellite Communications and Networking*, **41**, 158–177.

3

Validation routines

As part of the work presented in chapter 2, multiple validations routines were developed to ensure the validity of the results. First, the central positioning tool was verified and validated throughout development, and highlighted in section 3.1 are key tests for the proper functionality of the tool. Secondly, assumptions made on the variance of the rudimentary ground constraint in the positioning tool, and variance of the simulated GPS range measurements included in the analysis, are validated by way of sensitivity analysis, shown in section 3.2. Transparency in these validation routines gives further confidence in the results of the presented research.

3.1. Positioning validation

The performance of the positioning tool is validated using representative GPS measurements. Located well within the Arctic circle, the IGS station TRO100NOR[1] is centrally housed on the top of Tromsø island in Norway, where the station has been in operation since 1997, and receives various GNSS observations for the IGS network.

Pseudorange measurements are obtained from the ESA *GNSS Science Support Centre* (GSSC), accessible through the public *GSSC Now* interface. The data used for validation are GPS measurements generated at the TRO100NOR station on Nov 1st 2022, sampled every 30 s between 17:00 and 20:00. The measurements made at 18:00 are used for validating the point positioning functionality of the tool, and the measurements made by the *USA-232* GPS-satellite, identified by the pseudorandom noise (PRN) number 1, between 18:00 and 19:00 are used for demonstrating single-satellite navigation functionality.

Table 3.1: Details of the IGS TRO100NOR station.

STATION TRO100NOR	
Location	Tromsø, Norway
Latitude, Longitude	69.663, 18.940
Height	138.0 m

Figure 3.1: The location of TRO100NOR station in Tromsø, Norway.

The position of all GPS satellites in this timeframe are sampled from the final precise orbit products of the *International GNSS Service* (IGS). This data is accessed through the NASA *Crustal Dynamics Data Information System* (CDDIS)[2,3]. These highly accurate position estimates are only sampled every fifteen minutes, meaning the satellite positions must be interpolated over the chosen 3-hour time span using a cubic spline, implemented with the `scipy.interpolate.CubicSpline` method[4], with a

[1] URL https://www.igs.org/imaps/station.php?id=TRO100NOR, Accessed 3/10/2023.
[2] URL https://igs.org/products/, Accessed 3/10/2023.
[3] URL https://cddis.nasa.gov/, Accessed 3/10/2023.
[4] URL https://docs.scipy.org/doc/scipy/reference/generated/scipy.interpolate.CubicSpline.html, Accessed 3/10/2023.

”not-a-knot” boundary condition at both ends.

Positioning using the collected dual-frequency GPS pseudorange measurements are shown to fall within an expected accuracy. Standard dual-frequency GPS pseudorange observations error budgets have an expected error of 1.4 m, and a positioning solution can be considered validated if at a similar error level, yet higher due to geometric considerations (Kaplan & Hegarty, 2006, Tab. 7.3). The point positioning is performed by combining the coarse acquisition (C/A) pseudorange measurements ρ_1 with the associated L5-band pseudoranges ρ_2, for a corrected pseudorange measurement ρ_c, free of ionospheric time-delay. This is possible due to the different frequencies (f_1 = 1575.42 MHz, f_2 = 1176.45 MHz) of the two measured signals, combined in a ionosphere-free pseudorange as in Equation 3.1 by exploiting the inverse-square relationship between frequency and the time-delay due to the ionosphere (Tapley et al., 2004, Eq. 3.4.14 - 3.4.15). At the chosen time, 18:00 on Nov 1st 2022, there are six GPS satellites from which both C/A and L5-band pseudorange observations are observed at the TRO100NOR station. A light-time correction in the satellite position is required to find the satellite position at time of transmission, and because the GPS satellite positions are reported in an Earth-centered Earth-fixed (ECEF) frame, an additional correction for Sagnac delay is also applied to the pseudorange observation. The velocity of each satellite is found by the derivative of the cubic spline interpolation of the satellite positions. The resulting six ionosphere-free pseudorange measurements are used to validate the *functionality* of the point positioning tool, with a demonstrated absolute accuracy of 9.9 m. This error is on the expected level given the error budget, and demonstrates that the positioning tool can provide a receiver position estimate without introducing significant error. The positioning tool with its light-time and sagnac delay correction is thereby validated using empirical GPS data. The functionality of the light-time correction is validated using the same pseudorange measurements. The resulting point positioning accuracy is shown to decrease significantly when not including the light-time correction, with a demonstrated absolute accuracy of 29.9 m. This result validates the implementation of the light-time correction. The positioning accuracy did not significantly change when neglecting the Sagnac delay correction, which is believed to be due to the small change in the position of GPS satellites during time-of-flight of the signal. The functionality of the Sagnac delay was instead validated through the simulation of the Iridium constellation, evaluated as described in the methodology in chapter 2, but with an observation variance of 1 m and both with and without the Sagnac delay correction. The mean positioning error, when applying the Sagnac delay correction when not required, is shown to increase by 0.5 m from an otherwise near-perfect positioning result, which is equal to the value of the Sagnac delay range correction itself. This result validates the implementation of the Sagnac delay.

$$\rho_c = \frac{f_1^2}{f_1^2 - f_2^2}\rho_1 - \frac{f_2^2}{f_1^2 - f_2^2}\rho_2 \tag{3.1}$$

As the topic of positioning using only a single satellite is especially relevant for project ICING, additional validation of this concept is also performed. The pseudorange observations associated with a single random satellite, in thise case PRN 1, are combined with the interpolated position and velocity of the satellite over a whole hour, from 18:00 until 19:00. This results in 120 pseudorange observations provided to the positioning tool as independent observations. The positioning algorithm was also run with a surface constraint which is implemented as a range measurement equal to the norm of the position of the receiver relative to the center of the Earth, including a low measurement variance of 1.0 m to provide a relatively high weight to the constraint in the least-squares estimation. The result is the successful validation of the point positioning *functionality* using only a single satellite, both without and with a ground constraint, with a resulting absolute accuracy of 2037.5 m and 197.9 m, respectively. The resulting observation residuals are shown in Figure 3.2 as a function of time through this hour.

Table 3.2: The impact on the mean surface position error when using varying ground constraint standard deviations for the single-satellite rolling performance and the Iridium constellation.

Std. dev. [m]	Iridium pos. err. [m]	Rolling perf. [m]
1.0*	337.5	18124.4
10.0	335.5	18407.1
100.0	335.5	18534.6
1000.0	335.5	18534.8
10000.0	335.5	18534.8

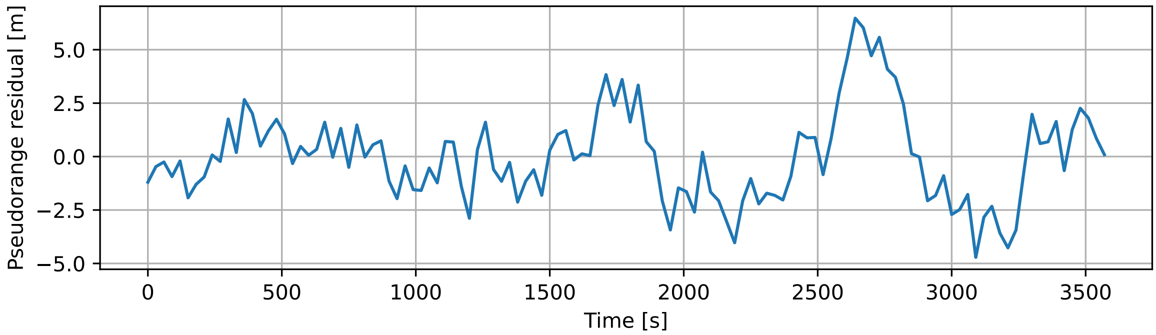

Figure 3.2: The pseudorange residuals after positioning using a single GPS satellite, presented as a function of time through the pass.

3.2. Sensitivity analysis

Parts of the method of the journal article in chapter 2 rely on particularly assumed variance levels for a weighted positioning estimate. This section will present a validation by way of a sensitivity analysis of the results with respect to these assumed variance levels. First, the chosen 1 m variance of the implemented ground constraint is validated in subsection 3.2.1. Secondly, the chosen 4 m variance in the simulated GPS range measurements is validated in subsection 3.2.2.

3.2.1. Ground constraint variance

The method of the journal article describes the use of a rudimentary ground constraint. This ground constraint was implemented as a pseudorange observation from the center of the Earth, with the measured range equal to the true range to the receiver. In this way, the positioning solution is constrained to approximately the geoid surface at the receiver. This constraint is not a realistic implementation, but the development of a more sophisticated geoid-constrained problem is beyond the scope of this analysis. The rudimentary approach was implemented with key assumptions on its inherent variance in the positioning solution. The ground constraint pseudorange was assumed a variance of 1.0 m, meaning the weighted observation residuals would give a larger weight to the ground constraint compared to the VDES observations, which had a standard deviation of 260.8 m. It is of interest to show that using a larger standard deviation of the ground constraint does not considerably effect the results of the analysis.

As is clear from the results of the journal article in chapter 2, the OneWeb constellation does not significantly improve with the addition of a ground constraint. In that regard, only the choice of the ground constraint variance for the Iridium constellation and the rolling performance of the single satellite be must be validated. The variance is increased from 1 m, that is used in the analysis of the journal article, exponentially to a standard deviation of 10000 m. The validation of the Iridium constellation results are done by ensuring the mean surface position error will not vary significantly with an increased ground constraint variation. In the case of the rolling performance, the sum of the surface positioning errors using each whole pass is inspected for significant impact of a varying ground constraint variation.

It is clear from the results in Table 3.2 that the results do not considerably change with a more un-

*The standard deviation used in the journal article.

Table 3.3: The change in the mean and standard deviation of the surface position error with an increasing GPS range variance, in the analysis of NorSat-TD as a contemporary backup service.

GPS range st. dev. [m]	Mean surface pos. err. [m]	St. dev. surface pos. err. [m]
4.0*	218.2	212.4
8.0	218.9	212.0
16.0	222.7	213.4
32.0	232.7	212.8
64.0	260.6	215.7

certain ground constraint. First, the position estimation error is largely unaffected, and even decreased slightly with the first iteration of increasing the ground constraint variance. The position error for the rolling performance shows a slight degradation, but plateau for large increases in the ground constraint variance. Not shown in the table, the result that six of the eleven passes result in a surface position error below 1 km, also remains valid for increasing ground constraint variance. With these results, it is clear that the assumption for the variance of the ground constraint does not considerable affect the accuracy of the positioning results, and thus the conclusions of the journal article.

3.2.2. GPS range signal variance

To evaluate the performance of a contemporary contingency system using NorSat-TD and only partial GNSS coverage, GPS range measurements were simulated as part of the work in the journal article in chapter 2. These range measurements were evaluated as the perfect geometric range between interpolated GPS positions and the known receiver position, with added Gaussian noise. The normally distributed error contribution was given a variance of 4 m, based on published GPS error budgets for single-frequency users (U.S. Department of Defense, 2020). This has also been shown to be a conservative estimate of the ranging error of GPS for the modern system (Montenbruck et al., 2018). It is of interest to show that the results of the journal article do not vary when different GPS range errors are used.

This analysis will consider the change in the mean and standard deviation of the resulting surface position error of the simulated contingency system. These are the leading metrics supporting the conclusions of the article, which is that the accuracy of the contingency system, composed of three GPS observations and one VDE-SAT observation, is sufficiently below 1 km. The positioning results could vary because of the increased random noise of the GPS range observations, and also because of the change in the weights used for the positioning tool. However, the geometric filter is not influenced at all by the signal variance, so these results are not included in Table 3.3. Similarly, the studentized filter did not considerably affect the conclusions in the journal article, and will be therefore also not be considered here.

Table 3.3 shows that the results are not considerably influenced by an increase in the range variance of the simulated GPS signals. The mean surface position error only starts to increase significantly for unrealistically high error levels for the GPS range observations. Further, the standard deviation of the same error remains largely unchanged. With these results, it shown that the chosen noise level of the simulated GPS range measurements does not significantly affect the surface position error results, and thus the conclusions of the journal article.

*The standard deviation used in the journal article.

4 Conclusion and Outlook

The conclusions of the thesis work is shortly summarised in section 4.1, largely as a reflection of the journal article conclusions. Further, this chapter will present an outlook in the form of recommendations for further work in section 4.2. These recommendations are rooted in the conclusions of the journal article and the unanswered questions of the research proposal.

4.1. Conclusion

This thesis project set out to exploit the unique opportunity after the launch of NorSat-TD to join project ICING and get a first look at empirical VDE-SAT range measurements. The presented work has been centred around a journal article submission, with its own research goals and conclusions. A first analysis of the characteristics of empirical VDE-SAT range measurements was presented. This has given a new understanding of the error behaviour of VDE-SAT pseudoranges, by analysing the previously neglected signal propagation error. The largest propagation error was further suggested as likely being due to the time-delay due to the ionosphere, in line with hypotheses from recent literature. The article goes on to conclude on a positive feasibility of a future VDE-SAT general navigation backup system for application on the ocean, rooted in the contemporary performance of the system which shows positioning using a single satellite through a pass, as well as positioning using medium-size constellations can provide positioning accuracy within 1000 m. Limitations to this conclusion are also presented, highlighting the need for an autonomous positioning and timing synchronization to remove critical GNSS dependency before the system can successfully serve as a GNSS backup system. Finally, the research presents the opportunity to use VDE-SAT as a contemporary GNSS contingency system for a limited application, namely the combination of three GNSS observations and one VDE-SAT observation in a multi-source position estimation with occasional availability and accuracy within 1000 m. Recommendations are given on the further development of such a system, once again with a critical view at the current GNSS dependency of VDES.

4.2. Further work

Recommended as further work in the journal article is to expand on the applied analysis of a possible contingency system. The presented analysis is limited to the specific scenario of partial GNSS coverage with exactly three GPS and one VDE-SAT observation. The conclusion can not conclusively state that a contingency system can be implemented using the currently available technology, as the method is limited to only the specific scenario of combining three GPS and one VDE-SAT observations in a position estimate. Nevertheless, the results indicate that such a system has the potential to be used as a contemporary GNSS contingency system if certain areas of improvement are addressed. Primarily, the method can improved by including a wider and more realistic scope of geometries, with a varying number of GNSS and VDE-SAT observations. In particular, it is recommended to combine a partial GNSS coverage of also a single, and two available GNSS satellites, with multiple VDE-SAT observations through a pass. Further, the analysis can be extended to simulations of small constellations of VDE-SAT satellites, an example of which is shown in Figure 4.1, to evaluate the possible positioning

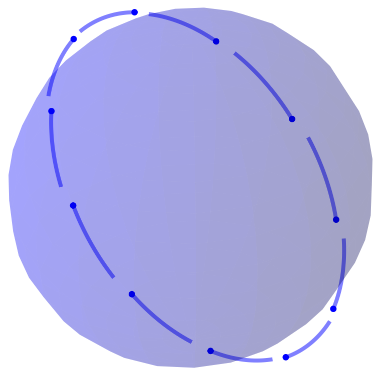

Figure 4.1: A small constellation of satellites in a polar orbit, providing continuous connection to a single satellite.

accuracy, as well as the required amount of satellites for a continuously operating GNSS contingency system in the Arctic.

The current study is conducted with a simple implementation of a least-squares estimate of the receiver position. Further study and performance analyses could benefit from more complex positioning methods. First, it is recommended to work on a dynamic parameter estimation method, as it build on the presented least-squares method, and is believed to be particularly applicable to maritime systems. When including the dynamics of a receiver in the parameter estimation, the elements of the design matrix $\mathbf{H}$ also include the time-variation of the receiver state, so that the time-derivative of the pseudoranges ρ become $d\rho/dt = \mathbf{f}(t, \mathbf{x}, \theta)$, with the receiver state $\mathbf{x}$ and a vector of dynamic parameters θ. This set of differential equations can be expanded to what is known as the *variational equations* of the problem, seen in Equation 4.1. The solution of these equations is the gradient $\partial\rho(t, \theta)/\partial\theta$, which as for a regular least-squares solution can be solved for an optimal set of dynamic parameters θ. These can, for example, be the navigational parameters of a ship at sea, its heading and speed, making it particularly applicable to the maritime domain where these parameters are typically constant over longer periods of time.

$$\frac{d}{dt}\frac{\partial\rho}{\partial\theta} = \frac{\partial\mathbf{f}}{\partial\rho}\frac{\partial\rho}{\partial\mathbf{x}} + \frac{\partial\mathbf{f}}{\partial\theta} \tag{4.1}$$

One limitation of the presented research was the investigation into the effects of known error sources. The work was limited by equipment and time to considering only the effect of time-delay due to the ionosphere on the range measurements. While this was a reasonable constraint, rooted in recent literature, it leaves the question open on what the influence of other common errors sources are on the observations. Other mentioned errors, that were not considered in the article, are receiver and transmitter clock jitter and drift in GNSS-down holdover periods, the observation noise, ephemeris errors, multipath errors, and other atmospheric effects, most notably the tropospheric time-delay. These are common sources of error that are typically considered in GNSS applications (Milliken & Zoller, 1978). Of these, it is recommended to further investigate the effect of the troposphere and multipath errors on VDE-SAT range measurements, as these have been previously hypothesised as the most critical sources of error after the ionosphere (Owens et al., 2021; Šafář et al., 2021).

There are multiple methods for investigating these effects in modern literature. The troposphere, unlike the ionosphere, is a non-dispersive medium for radio frequencies and as a result, the time-delay due to the troposphere will be similar to that experienced by GNSS. It is therefore recommended to take an approach to tropospheric correction techniques as available in literature for GNSS, as was done for ionospheric correction techniques in this work. Specifically, the model of Saastamoinen, 2013, in part used as the tropospheric correction model in the Galileo system, and modern IGS tropospheric products could be compared to investigate the influence on measured pseudoranges (Hackman et al., 2015). Further, multipath errors can be investigated using more sophisticated measurement techniques, as small and zero baseline measurements, with a combination of single- and double-differencing range measurements, which can be used to quantify code multipath delay (de Bakker et al., 2009). However, such methods require a larger investment in ground infrastructure, and later also in a larger constellation of satellites for a complete analysis. It is recommended to first investigate the influence of the troposphere, as this is possible with the current available infrastructure.

Bibliography

Aquino, M., Rodrigues, F. S., Souter, J., Moore, T., Dodson, A., & Waugh, S. (2005). Ionospheric scintillation and impact on GNSS users in Northern Europe: Results of a 3 year study. *Space Communications*, *20*(1-2), 17–29.

Kaplan, E. D., & Hegarty, C. (Eds.). (2006). *Understanding GPS: Principles and applications* (2nd ed). Artech House.

Reid, T., Walter, T., Blanch, J., & Enge, P. (2016). GNSS Integrity in The Arctic: GNSS Integrity in The Arctic. *Navigation*, *63*(4), 469–492.

De Jong, K., Goode, M., Liu, X., & Stone, M. Precise GNSS Positioning in Arctic Regions. In: In *All Days*. Houston, Texas: OTC, 2014, February, OTC–24651–MS.

IALA. (2012b, December). R0129 GNSS VULNERABILITY AND MITIGATION MEASURES, Edition 3.1.

Maine, K., Devieux, C., & Swan, P. Overview of IRIDIUM Satellite Network. In: In *Wescon/95: Microelectronics, communications technology, producing quality products, mobile and portable power, emerging technology*. Piscataway, NJ: IEEE Service Center, 1995.

de Selding, P. B. (2015). Virgin, Qualcomm Invest in OneWeb Satellite Internet Venture. *Space News*.

Reid, T. G., Walter, T., Enge, P. K., Lawrence, D., Cobb, H. S., Gutt, G., O'Connor, M., & Whelan, D. Navigation from Low Earth Orbit: Part 1: Concept, Current Capability, and Future Promise. In: In *Position, Navigation, and Timing Technologies in the 21st Century*. Wiley, 2020, December, pp. 1359–1379.

IALA. (2019, June). G1139 THE TECHNICAL SPECIFICATION OF VDES, Edition 3.

ITU-R. (2022, February). Recommendation ITU-R M.2092-1: Technical characteristics for a VHF data exchange system in the VHF maritime mobile band.

Sheng-Ju, S. Implementation of Cyclic Redundancy Check in Data Communication. In: In *2015 International Conference on Computational Intelligence and Communication Networks (CICN)*. Jabalpur, India: IEEE, 2015, December, 529–531.

Lázaro, F., Raulefs, R., Wang, W., Clazzer, F., & Plass, S. (2019). VHF Data Exchange System (VDES): An enabling technology for maritime communications. *CEAS Space Journal*, *11*(1), 55–63.

Kang, T., Li, X., Yu, C., & Kim, J. (2013). A Survey of Security Mechanisms with Direct Sequence Spread Spectrum Signals. *Journal of Computing Science and Engineering*, *7*(3), 187–197.

Kapoor, R., Ramasamy, S., Gardi, A., & Sabatini, R. (2017). UAV Navigation using Signals of Opportunity in Urban Environments: A Review. *Energy Procedia*, *110*, 377–383.

Jia, M., & Kassas, Z. M. (2022). Kalman Filter-Based Integrity Monitoring for GNSS and 5G Signals of Opportunity Integrated Navigation. *IFAC-PapersOnLine*, *55*(24), 273–278.

Kassas, Z. M., Khalife, J., Abdallah, A., Lee, C., Jurado, J., Wachtel, S., Duede, J., Hoeffner, Z., Hulsey, T., Quirarte, R., & Tay, R. (2022). Assessment of Cellular Signals of Opportunity for High-Altitude Aircraft Navigation. *IEEE Aerospace and Electronic Systems Magazine*, *37*(10), 4–19.

IALA. (2012a, December). IALA World Wide Radio Navigation Plan, Edition 2.

Johnson, G., & Swaszek, P. (2014, August). Feasibility Study of R-Mode using AIS Transmissions.

Hu, Q., Jiang, Y., Zhang, J., Sun, X., & Zhang, S. (2015). Development of an Automatic Identification System Autonomous Positioning System. *Sensors*, *15*(11), 28574–28591.

Gewies, S. (2018, May). R-Mode Testbed in the Baltic Sea.

Šafář, J., Grant, A., Williams, P., & Ward, N. (2020). Performance Bounds for VDES R-mode. *Journal of Navigation*, *73*(1), 92–114.

Wirsing, M., Dammann, A., & Raulefs, R. Investigating R-Mode Signals for the VDE System. In: In *OCEANS 2019 MTS/IEEE SEATTLE*. Seattle, WA, USA: IEEE, 2019, October, 1–5.

Šafář, J., Grant, A., & Bransby, M. (2021). Performance bounds for VDE-SAT R-Mode. *International Journal of Satellite Communications and Networking*, (Special issue paper).

Šafář, J., Shaw, G., Grant, A., Haugli, H. C., Løge, L., Christiansen, S. E., & Alagha, N. GNSS Augmentation using the VHF Data Exchange System (VDES). In: In *31st International Technical Meeting of The Satellite Division of the Institute of Navigation (ION GNSS+ 2018)*. Miami, Florida, 2018, October, 1788–1805.

Owens, A. J., Richardson, T., & Critchley-Marrows, J. The Feasibility of a VDE-SAT Ranging Service as an Augmentation to GNSS for Maritime Applications. In: In *34th International Technical Meeting of the Satellite Division of The Institute of Navigation (ION GNSS+ 2021)*. St. Louis, Missouri, 2021, October, 591–616.

Tapley, B. D., Schutz, B. E., & Born, G. H. (2004). *Statistical orbit determination*. Elsevier Academic Press.

U.S. Department of Defense. (2020, April). *GLOBAL POSITIONING SYSTEM STANDARD POSITIONING SERVICE PERFORMANCE STANDARD* (tech. rep.). U.S. Department of Defense.

Montenbruck, O., Steigenberger, P., & Hauschild, A. (2018). Multi-GNSS signal-in-space range error assessment – Methodology and results. *Advances in Space Research*, *61*(12), 3020–3038.

Milliken, R. J., & Zoller, C. J. (1978). Principle of Operation of NAVSTAR and System Characteristics. *Navigation*, *25*(2), 95–106.

Saastamoinen, J. Atmospheric Correction for the Troposphere and Stratosphere in Radio Ranging Satellites. In: In *Geophysical Monograph Series*. Washington, D. C.: American Geophysical Union, 2013, March, pp. 247–251.

Hackman, C., Guerova, G., Byram, S., Dousa, J., & Hugentobler, U. International GNSS Service (IGS) Troposphere Products and Working Group Activities. In: In *From the Wisdom of the Ages to the Challenges of the Modern World*. Sofia, Bulgaria, 2015, May.

de Bakker, P. F., van der Marel, H., & Tiberius, C. C. J. M. (2009). Geometry-free undifferenced, single and double differenced analysis of single frequency GPS, EGNOS and GIOVE-A/B measurements. *GPS Solutions*, *13*(4), 305–314.